

Challenges in conditioning a stochastic geological model of a heterogeneous glacial aquifer to a comprehensive soft dataset.

Julian Koch^{1,2,*}, Xin He², Karsten Høgh Jensen¹, Jens Christian Refsgaard²

¹Department of Geosciences and Natural Resource Management, University of Copenhagen

²Department of Hydrology, Geological Survey of Denmark and Greenland

Submitted to:

HESS – Hydrology and Earth System Sciences

*Corresponding Author Address:

Julian Koch

Department of Hydrology

Geological Survey of Denmark and Greenland (GEUS)

Øster Voldgade 10

Copenhagen, Denmark

E-mail: juko@geus.dk

Telephone: +45 38142768

16 Abstract

17 In traditional hydrogeological investigations, one geological model is often used based on subjective
18 interpretations and sparse data availability. This deterministic approach usually does not account for any
19 uncertainties. Stochastic simulation methods address this problem and can capture the geological structure
20 uncertainty. In this study the geostatistical software TProGS is utilized to simulate an ensemble of
21 realizations for a binary (sand/clay) hydrofacies model in the Norsminde catchment, Denmark. TProGS
22 can incorporate soft data, which represent the associated level of uncertainty. High density (20m x 20m x
23 2m) airborne geophysical data (SkyTEM) and categorized borehole data are utilized to define the model
24 of spatial variability in horizontal and vertical direction, respectively and both are used for soft
25 conditioning the TProGS simulations. The category probabilities for the SkyTEM dataset are derived
26 from a histogram probability matching method, where resistivity is paired with the corresponding
27 lithology from the categorized borehole data. This study integrates two distinct datasources into the
28 stochastic modeling process that represent two extremes of the conditioning density spectrum; sparse
29 borehole data and abundant SkyTEM data. In the latter the data has a strong spatial correlation caused by
30 its high data density, which triggers the problem of overconditioning. This problem is addressed by a work
31 around utilizing a sampling/decimation of the dataset, with the aim to reduce the spatial correlation of the
32 conditioning dataset. In the case of abundant conditioning data it is shown that TProGS is capable of
33 reproducing non-stationary trends. The stochastic realizations are validated by five performance criteria:
34 (1) Sand proportion, (2) mean length, (3) geobody connectivity, (4) facies probability distribution and (5)
35 facies probability – resistivity bias. As conclusion, a stochastically generated set of realizations soft
36 conditioned to 200m moving sampling of geophysical data performs most satisfying when balancing the
37 five performance criteria. The ensemble can be used in subsequent hydrogeological flow modeling to
38 address the predictive uncertainty originated from the geological structure uncertainty.

39 Key words: Geological model, stochastic simulation, geophysical data, soft conditioning, model
40 performance, TProGS

1. Introduction

Constraints in accurate and realistic solute transport modeling in hydrogeology are caused by the difficulty of characterizing the geological structure. The subsurface heterogeneity heavily influences the distribution of contaminants in the groundwater system. The scale of heterogeneity is often smaller than the data availability (e.g. borehole spacing). In traditional hydrogeological studies, one geological model is built based on the best comprehensive knowledge from often sparse borehole data and subjective interpretations. This can lead to alleged correct results, for instance when addressing the water balance on catchment scale, but will often prove to be inadequate for simulations beyond general flows and heads, e.g. contaminant transport modeling. Therefore, it is proposed by numerous studies that the uncertainty on the geological conceptualization is crucial when assessing uncertainties on flow paths (Neuman, 2003; Bredehoeft, 2005; Hojberg and Refsgaard, 2005; Trolborg et al., 2007; Seifert et al., 2008). One of the strategies often recommended for characterizing geological uncertainty and assessing its impact on hydrological predictive uncertainty is the use of multiple geological models (Renard, 2007; Refsgaard et al., 2012).

In this respect geostatistical tools such as two-point statistics e.g. TProGS (Carle and Fogg, 1996; Carle et al., 1998) and multipoint statistics (MPS) (Caers and Zhang, 2002; Strebelle, 2002; Caers, 2003; Journel, 2004) are powerful tools as they enable the generation of multiple equally plausible realizations of geological facies structure. This study targets the realistic description of heterogeneity in a geological model by introducing diverse data into the stochastic modeling process to generate a set of equally plausible realizations of the subsurface using geostatistics (Refsgaard et al., 2006).

61 In geostatistical applications field observations can constrain the simulation as soft or hard conditioning.
62 “Hard conditioning” forces the realizations to honor data completely whereas “soft conditioning” honors
63 the data partly with respect to the uncertainty of the observation (Falivene et al., 2007). This feature is
64 essential because it enables the user to associate uncertainties to the conditioning dataset that can be of
65 either subjective or objective nature. Incorporating a comprehensive and continuous soft conditioning
66 datasets to a stochastic simulation such as TProGS is challenging. Alabert (1987) published an early study
67 on the implications of using sparse soft conditioning data to a stochastic simulation. The analysis shows
68 that soft conditioning significantly increases the quality of the realizations. The same was also observed
69 by McKenna and Poeter (1995) where soft data from geophysical measurements could significantly
70 improve the geostatistical simulation. In the past years, highly sophisticated geophysical methods and
71 advanced computational power allow stochastic simulations that are conditioned to a vast auxiliary
72 dataset. This poses new challenges to the data handling and to the simulation techniques.

73 Chugunova and Hu (2008) present a study where continuous auxiliary data is introduced directly, without
74 classification to a MPS simulation data in addition to the general training image. MPS requires a site
75 specific training image that represents the geological structure accordingly, which is often the main
76 source of uncertainty in MPS simulations. The above mentioned MPS studies conduct mostly 2D
77 simulations, partly on synthetic data. The training image is the backbone of the MPS method and it has
78 been acknowledged by dell'Arciprete et al. (2012) and He et al. (2013) that reliable 3D training images
79 are difficult to acquire.

80 Alternative methods to integrate vast auxiliary information (e.g. geophysics) into the modeling process
81 and at the same time force local accuracy are collocated cokriging or cosimulation techniques (Babak and

82 Deutsch, 2009). Here a linear relationship between the auxiliary variable and the target variable is built in
83 a model of cross covariance. The essentially linear relationship is often too restrictive and does not
84 represent the complex physical processes. Mariethoz et al. (2009b) present a prospective method that
85 extends the collocated simulation method by using a model of spatial variability of the target variable and
86 a joint probability density distribution to depict the conditional distribution of the target variable and the
87 auxiliary variable at any location.

88 The method of anchored distributions (MAD) (Rubin et al., 2010) is a suitable approach for the inverse
89 modeling of spatial random fields with conditioning to local auxiliary information. Structural parameters
90 such as global trends and geostatistical attributes are considered in a conditional simulation. The
91 conditioning is undertaken by anchored distributions which statistically represent the relationship between
92 any data and the target variable.

93 The truncated plurigaussian simulation method (Mariethoz et al., 2009a) generates a Gaussian field for
94 the target and the auxiliary variable using variogram statistics. These Gaussian fields are truncated to
95 produce categorical variables that represent the hydrofacies. The truncation is controlled by threshold
96 values that can be defined in a “lithotype rule” that represents the general geological concept. It is a very
97 flexible method, because conceptual understandings are easily incorporated, but non-stationarity and
98 especially directional depended lithotype rules are difficult to incorporate.

99 TProGS is a well-established stochastic modeling tool for 3D applications and it has been successfully
100 applied to simulate highly heterogeneous subsurface systems by constraining the simulation to borehole
101 data (Carle et al., 1998; Fleckenstein et al., 2006). Weissmann et al. (1999), Weissmann and Fogg (1999)

102 and Ye and Khaleel (2008) use additional spatial information obtained from soil surveys, sequence
103 stratigraphy and soil moisture, respectively for accessing the complex lateral sedimentary variability and
104 thus improving the quality of the model in terms of spatial variability. It has not been tested whether
105 TProGS, is capable of handling abundant soft conditioning data. Moreover, the risk that a cell-by-cell soft
106 constraining may cause an overconditioning of the simulation has not been fully investigated.
107 Overconditioning is defined by the authors as an effect triggered by dense and spatial correlated
108 conditioning data that produces an altered picture of observable uncertainties. Therefore the self-
109 consistency of the stochastic simulation is questioned, because soft constraining should be treated
110 accordingly during the simulation.

111 Recent studies by Lee et al. (2007) and dell'Arciprete et al. (2012) highlight that TProGS is comparable
112 with other geostatistical methods like, multi-point statistics, sequential Gaussian simulations and
113 variogram statistics (Gringarten and Deutsch, 2001). The distinct strength of TProGS is the simple and
114 direct incorporation of explicit facies manifestations like mean length, proportion and (asymmetric)
115 juxtapositional tendencies of the facies.

116 Geophysical datasets are valuable information in many hydrogeological investigations. It can
117 considerably improve the conceptual understanding of a facies or hydraulic conductivity distribution and
118 identify non-stationary trends. However, the integration of geophysical data and lithological borehole
119 descriptions is often difficult. A recent study by Emery and Parra (2013) presents an approach to combine
120 borehole data and seismic measurements in a geostatistical simulation to generate multiple realizations of
121 porosity. Hubbard and Rubin (2000) review three methods that allow hydrogeological parameter
122 estimation based on geophysical data. The three methods link seismic, ground penetrating radar (GPR)

123 and tomographic data with sparse borehole data to support the hydrogeological description of the study
124 site. Our study integrates high resolution airborne geophysical data with borehole data to build a
125 probabilistic classification of the subsurface at site. The geophysical data are collected by SkyTEM, an
126 airborne transient electromagnetic method (TEM) that has been used extensively in Denmark for the
127 purpose of groundwater mapping (Christiansen and Christensen, 2003; Jorgensen et al., 2003b; Sorensen
128 and Auken, 2004; Auken et al., 2009). This study utilizes a method that translates SkyTEM observation
129 data into facies probability which enables associating the geophysical data with softness, according to the
130 level of uncertainty. Very few studies have integrated high resolution airborne geophysical data in a
131 stochastic modeling process (Gunnink and Siemon, 2009; He et al., 2013).

132 Most stochastic studies only make relatively simple validations of how well the simulations are able to
133 reproduce known geostatistical properties. Carle (1997) and Carle et al. (1998) investigate the goodness
134 of fit between the simulated and the defined model of spatial variability. The geobody connectivity is
135 used by dell'Arciprete et al. (2012) to compare results originated from two- and multipoint geostatistics.
136 Chugunova and Hu (2008) make a simple visual comparison between the auxiliary variable fracture
137 density and stochastic realizations of the simulated fracture media. A more advanced validation is
138 conducted by Mariethoz et al. (2009b) where simulated variograms and histograms are compared with
139 reference data for the simulation of synthetic examples. In spite of these few studies that have addressed
140 the validation issue, no guidance on which performance criteria to use and how to conduct a systematical
141 validation of a stochastic simulation has been reported so far.

142 It should be noted that we in line with Refsgaard and Henriksen (2004) do not use the term model
143 validation in a universal manner, but in a site specific context where a model validation is limited to the

144 variables for which it has been tested as well as to the level of accuracy obtained during the validation
145 tests.

146 The objectives of this study are: (1) to set up TProGS for a study site based on lithological borehole data
147 and high resolution airborne geophysical data and investigate the effect of the two distinct conditioning
148 datasets to the simulation; (2) to assess the problem of overconditioning in a stochastic simulation; (3) to
149 ensure that non-stationary trends are simulated accordingly by TProGS; and (4) to identify and test a set
150 of performance criteria for stochastic simulations that allow the validation against geostatistical properties
151 derived from field data. The results of the present study are intended for application in a hydrological
152 modeling context (Refsgaard et al., 2014), where the geological uncertainty, represented by a set of
153 plausible realizations of the subsurface, is propagated through the model. The varying flowpaths between
154 the realizations will affect solute transport and thus nitrate reduction and can be utilized to assess the scale
155 of potential predictive capability of the hydrogeological flow model.

156 2. Study Site

157 Figure 1 shows the 101 km² Norsminde catchment, located on the east coast of Jutland south of Aarhus.
158 The topography allows a separation between an elevated western part, with changing terrain and a
159 maximum elevation of 100 m and a flat and low elevated eastern part, where the coastline represents the
160 eastern boundary. Glacial morphologies, namely moraine landscapes are predominant in most of the
161 catchment. The geological stratigraphy indicated by borehole logs encompasses Paleogene and Neogene
162 marine sediments underlying a heterogeneous stratigraphy of Pleistocene glacial deposits. The Paleogene
163 sediments are characterized by very fine-grained impermeable marl and clay. Above the Neogene
164 sequence shows sandy formations encased by a clay-dominated environment with Miocene marine
165 sediments. The entire Miocene sequence varies in thickness up to 40 m and the sandy formations reach
166 thicknesses of more than 10 m. The Miocene sequence is only present in the western part of the
167 catchment where the stochastic modeling is conducted and forms the lower boundary of the simulation
168 domain. Thus, only the upper Pleistocene glacial sequence is modeled. The glacial deposits in the western
169 part of the catchment contain both sandy and clayey sediments, where clay is predominant. Borehole logs
170 indicate that the Pleistocene clay spans from glaciolacustrine clay to clay till. Within the clay
171 environment, the sandy units are allocated in small units and vary between gravel, meltwater-sand and
172 sandy tills. The total thickness of glacial sediments varies between 10 and 40 m with heterogeneous
173 distributions of the mostly glaciofluvial sand features between less than a meter and 20 m in thickness.
174 The subject to the stochastic modeling, the delineated Pleistocene glacial sequence in the western part,
175 provides interesting challenges like distinct heterogeneity and a diverse terrain.

176 3. Data

177 Two different sources of data, namely lithological borehole data and airborne based geophysical data
178 (SkyTEM) are used, where the former is utilized to describe the vertical sand and clay variability and the
179 latter for assessing the lateral direction.

180 3.1. Borehole Data

181 The borehole dataset contains 112 borehole logs with varying depths. The descriptions in the borehole
182 reports are converted to a categorical binary (sand/clay) system at 5 cm vertical discretization. Further
183 each borehole's uncertainty is validated according to the method of He et al. (2014). The uncertainty
184 assessment allows defining individual trust scores and thus the definition of how much each borehole
185 should constrain the conditional simulation in the form of soft data. Drilling method, age, purpose of
186 drilling, among others are used as variables to ensure a systematic approach to validate the uncertainty of
187 each individual borehole. The boreholes are grouped into four quality groups with 100%, 95%, 90% and
188 85% as trust scores. The classified borehole dataset states an overall sand proportion of 30%.

189 3.2. Geophysical Data

190 The geophysical dataset comprises resistivity data from SkyTEM helicopter surveys. The SkyTEM
191 method has been extensively used for subsurface mapping in Denmark (Jorgensen et al., 2003a;
192 Jorgensen et al., 2005), where it has proven to be a successful tool for hydrogeological investigations.
193 SkyTEM data have the advantage of a high spatial resolution in the top 20 to 30m and at large spatial
194 coverage. However, some studies rise concern about the accuracy of interpretations of deep soundings
195 (Andersen et al., 2013). In the Norsminde catchment data were collected at 2000 flight km containing
196 over 100,000 sounding points. The distance between the flight lines is between 50 and 100 m. The
197 dataset is processed with a spatially constrained inversion algorithm (Schamper and Auken, 2012)
198 giving a 3D distribution of the underground resistivity. The sounding data were interpolated to a 20m x
199 20m x 2m grid domain by using 3D kriging as the interpolation method. The gridded resistivity data can
200 be utilized as a proxy for lithology, as high and low resistivity cells indicate a high probability of sand

and clay, respectively. Bowling et al. (2007) conduct a detailed study on the relationship between sediment and resistivity at a field site. Resistivity is linked to grainsize distribution and is used to delineate mayor geological structures. A strong positive correlation between gravel content in the lithology and resistivity is observed.

The SkyTEM dataset covers approximately 85% of the delineated glacial sequence. Figure 2 shows the spatial variation of the median resistivity for a 4- and a 16- subarea grid. Higher median resistivity values are located in the southern part of the glacial sequence. This indicates a greater sand proportion in the given areas. The conclusion of the spatial pattern in Figure 2 is that stationarity cannot be attested to the glacial sequence. This will have implications for the stochastic simulation.

The exact sand proportion can be derived by introducing a cut off value that divides the SkyTEM dataset into a sand and a clay fraction. Jorgensen et al. (2003b) estimate resistivity thresholds to differentiate between sediments in buried valleys in Denmark. Accordingly, glacial sand has a resistivity greater than 60 Ωm whereas clayey till sediments are placed between 25 and 50 Ωm and thus the exact cut off value varies between study sites.

3.3. Data integration

Figure 3 underlines some of the associated problems of the data integration of geophysical SkyTEM data and borehole descriptions. The lithological information from the borehole interprets thin layers of meltwater sand confined by clay in the top few meters. The SkyTEM data with a vertical resolution of two meters cannot capture this small scale variability. This supports to use geophysical data only for the lateral model of spatial variability and to incorporate the fine descriptions from the borehole data for the vertical model of spatial variability.

He et al. (2014) developed a method to manually calibrate the cut off value by comparing borehole with SkyTEM data at different spatial domains with the aim to reduce the deviation in sand proportion between the two data types. It is assumed that the deviation has to be minimized at domains with a high borehole density where the boreholes are assumed to best represent the domain conditions. It is shown

226 that a borehole density of 2 per km² reduces the representative error and that 46 Ωm as cut off value
227 reduces the deviation in sand proportion between the two datasets. The calibrated cut off value yields a
228 sand proportion of 23%.

229 Further He et al. (2014) developed a histogram probability matching (HPM) method that enables a direct
230 translation from resistivity into facies probability. Resistivity is paired with the lithological borehole
231 description at the coinciding cell. The data pairs are grouped in 10 Ωm bins and for each bin the sand/clay
232 fraction is first calculated and then plotted as a histogram. 3rd order polynomial curve fitting is applied to
233 the histogram and the manually calibrated cut off value is superimposed to the fitted curve (Figure 4). The
234 shape of the curve reflects the lumped uncertainties from both datasets. The flatness of the transition
235 zone, around 50%, sand probability indicates a high uncertainty for the corresponding resistivity values.
236 There are many sources of uncertainty that will affect the relationship between electrical conductivity and
237 facies information. The HPM-method lumps various sources and the shape of the fitted curve reflects
238 those, especially the width of the transition zone. He et al. (2014) discussed the prevalent uncertainties:
239 first, borehole descriptions are not accurate, and classification of borehole lithology is subjective. Second,
240 there are uncertainties on the resistivity data due to the resolution of the physics itself, the geophysics
241 instruments, field measurements and signal processing (inversion). Third, there is no unique relationship
242 between resistivity and lithology, and the curve can therefore be fitted in various ways. Last, there are
243 uncertainties related to the scale of aggregation, since the borehole data and geophysical data have
244 different resolutions and hence different supporting scales. The HPM-method used in this study is study
245 site specific and is purely based on spatial correlations and is not build up on physical relationships.
246 Therefore it cannot be transferred to other catchments, however the relationship between resistivity and
247 facies is manually calibrated for this site and is thus expected to be valid.

248 The HPM-method is a probabilistic approach and it is preferred to deterministic model
249 approaches, because of its suitability for soft conditioning in a stochastic geological simulation.
250 In a more deterministic sense, a positive correlation between resistivity soundings and hydraulic

251 conductivity estimates derived from pumping test has been acknowledged for glacial outwash
252 aquifers (Urish, 1981). Linde et al. (2006) review different strategies to relate geophysical and
253 hydrogeological properties and attest that geophysics undoubtedly add value to a
254 hydrogeological characterization. One suggested approach, which would be suitable for
255 SkyTEM data for the estimation of hydrogeophysical parameters, is the joint inversion, where
256 the geophysical or the hydrogeological inversion utilizes hydrogeological or geophysical data,
257 respectively. Another review paper by Slater (2007) address joint inversion methods as well as
258 petrophysical relations between geophysical (electrical) properties and effective hydraulic
259 properties (pore volume and pore surface) at core and field scale, which allow direct mapping of
260 hydraulic properties (Kemna et al., 2004). Slug tests with an estimate of the local saturated
261 hydraulic conductivity are available for the Norsminde catchment. However, due to differences
262 in scale, a low number of slug tests and unclarity of the correlation we found the direct mapping
263 approach unfeasible for our study.

264 4. Methods

265 4.1. TProGS – Transition Probability Geostatistical Software

266 The geostatistical software TProGS is applied in this study. It is based on the transition probability (TP)
267 approach (Carle and Fogg, 1996; Carle et al., 1998). Continuous Markov Chain models (MCM) are used
268 to represent the model of spatial variability (Krumbein and Dacey, 1969; Carle and Fogg, 1997; Ritzi,
269 2000). TProGS allows for the simulation of multiple realizations by utilizing a sequential indicator
270 simulation (SIS) (Seifert and Jensen, 1999) and by performing simulated quenching (Deutsch and
271 Cockerham, 1994; Carle, 1997). These two steps are mutually dependent and they make sure that the
272 realizations honor local conditioning data as well as the defined model of spatial variability.

273 The major advantage of TProGS is that fundamental observable attributes are parameterized in the
274 modelling process: volumetric fractions (proportions), mean lengths (thickness and lateral extent) and
275 (asymmetric) juxtapositional tendencies. These attributes can be assessed by data analysis and geological
276 interpretations and control the shape of the MCM model. The facies proportion is related to the
277 asymptotic limit of the MCM. The mean length is indicated on a plot of auto-transition probabilities as
278 the intersection of the tangent at the origin with the x-axis. Asymmetric juxtapositional tendencies are of
279 interest when simulating a system with at least three categories and can thus be neglected in this study.
280 TProGS computes the realizations of the geology in two uncoupled, but mutually dependent steps. An
281 initial configuration of facies distribution is produced by the SIS algorithm (Deutsch and Journel, 1992).
282 Secondly, the initial configuration is reshuffled by the simulation quenching optimization algorithm
283 (Deutsch and Cockerham, 1994). The TProGS simulation domain of this study is discretized into 20m x
284 20m x 2m cells on a 450 x 600 x 40 cell grid. The horizontal transition probabilities (TP) are based on
285 SkyTEM data, that is categorized by a cut off value of 46 Ω m and the vertical extent is purely based on
286 borehole data.

287 4.2. Split Sample Test

288 The two incorporated conditioning datasets are very distinct and will affect the simulation in opposite
289 ways: sparse borehole data allow large simulation freedom whereas dense SkyTEM data limit the
290 simulation freedom. Naturally they will be combined in order to condition the simulation to the best
291 combined knowledge of the system. However it is of interest to know how each individual conditioning
292 dataset affects the simulation. In this context a split sample test can reveal valuable information: one
293 simulation conditioning to purely borehole data and the other one conditioned to purely SkyTEM data. It
294 will be tested how well the simulations conditioned to borehole data reproduce the high resistivity cells,
295 where a high sand probability is evident and how well the simulations conditioned to SkyTEM data
296 reproduce the locations with borehole information.

297 4.3. Moving Sampling

298 Most studies on stochastic modeling condition the simulation to sparse data. In this study a
299 comprehensive cell-by-cell soft conditioning dataset is applied and it is anticipated that this may result in
300 overconditioning. Decimating the conditioning dataset out is a very intuitive sampling approach to work
301 around the problem of overconditioning. However, if the resampled conditioning dataset is too sparse,
302 information from the original dataset might not be sufficiently accounted for. Thus the tradeoff between
303 two extremes, too much and too few data is investigated. Opposed to the static sampling technique a
304 moving sampling method is applied. n different location grids with the same distance between the
305 samples for each chosen distance (100m, 200m, etc.), where each has an accumulated shift of the origin
306 (+ sampling distance/ n in X and Y direction). For the 100m moving sampling approach the first sampling
307 grid has the origin (0,0) the second (20,20), the third (40,40), etc. For the TProGS application in this
308 study five location grids are generated, which yields five independent soft conditioning datasets. Five
309 realizations are computed for each soft dataset; giving a total of 25 realizations. In addition to the
310 comparison between moving and static sampling, different sample densities are also be tested.

311 4.4. Sampling scenarios

312 In total, eight conditioning scenarios are tested in this study. For the split sample test two scenarios are
313 used, namely purely borehole data (*'onlyBH'*) and purely cell-by-cell SkyTEM data (*'onlySky20'*). In the
314 following both datasources are combined to represent the best combined knowledge of the system.
315 Further, static and moving sampling are applied: Borehole data and SkyTEM data sampled statically at
316 20m, 100m, 200m and 500m (*'BH-Sky20static'*, *'BH-Sky100static'*, *'BH-Sky200static'* and *'BH-*
317 *Sky500static'*, respectively). Moving sampling is tested at 100m and 200m sampling distance (*'BH-*
318 *Sky100moving'* and *'BH-Sky200moving'*, respectively).

319 4.5. Performance criteria

320 Five performance criteria are defined to evaluate an ensemble of realizations of the geology. They aim for
321 validating the ensemble with respect to the TProGS input, namely the defined model of spatial variability
322 (mean length and proportion) and the soft conditioning dataset. The five performance criteria test the self-
323 consistency of TProGS and thus if all input parameters and data are treated accordingly. The glacial
324 structure in the Norsminde catchment represents only approximately 20% of the entire TProGS
325 simulation domain and deviations in simulated spatial statistics between the entire model domain and the
326 simulation target are expected.

327 4.5.1. Sand proportion

328 The deviation between the mean simulated sand proportion and the defined sand proportion in the MCM
329 can be calculated for a set of realizations. The focus should be on the target area only, the area that will be
330 extracted from the rectangular model domain for subsequent applications. The analysis of the sand
331 proportion is based on 25 realizations.

332 4.5.2. Mean length

333 The simulated mean length can be estimated by recalculating the TPs from the TProGS output for the
334 target area only. The simulated TPs for a set of realizations can be averaged (10 realizations in this case)

335 and compared with the measured TPs to estimate the deviation in mean length between the predefined
336 and the mean simulated length.

337 4.5.3. Geobody connectivity

338 The degree of connectivity of permeable areas in the subsurface has major implications for flowlines and
339 particle ages. Renard and Allard (2013) conducted a methodology study on various static and dynamic
340 connectivity metrics. These metrics can be utilized as a comparison and interpretation indicator for
341 multiple stochastically generated realizations of the geology. The work by dell'Arciprete et al. (2012)
342 shows the successfully implementation of connectivity metrics to compare stochastic realizations
343 computed by two- and multi-point statistics. Giudici et al. (2011) underline that evidence of a single
344 “best” connectivity metric is still missing and further research is necessary in that field.

345 For this study two static connectivity metrics, θ and Γ , are selected. They refer to the first and second
346 geobody connectivity defined by Hovadik and Larue (2007). A geobody is defined as one connected 3D
347 cluster of sand. Hence it is a distinct sand feature that is confined by clay. The architectural elements are
348 interpreted on a 20m x 20m x 2m scale.

$$349 \quad \theta = \frac{V_l}{\sum_{i=0}^n V_i} \quad \text{Eq.1}$$

$$350 \quad \Gamma = \frac{\sum_{i=0}^n (V_i)^2}{(\sum_{i=0}^n V_i)^2} \quad \text{Eq.2}$$

351 where V_i is the volume of an individual geobody, n is the number of unconnected geobodies and V_l is the
352 volume of the largest occurring geobody. θ represents the ratio of the volume of the largest geobody to
353 the total volume. Denoted as Γ is the proportion of the pairs of cells that are connected among the entire
354 pairs. The two selected connectivity metrics originate from the percolation theory, which describes the
355 transition from many disconnected clusters to one large coherent cluster. This is mainly depending on the
356 facies proportion. As the proportion gradually increases it reaches a point where one big cluster appears.

357 The percolation threshold is expected to be approximately 0.59 and 0.31 for a 2D and 3D grid,
358 respectively (Hovadik and Larue, 2007). Mean values of θ and Γ are computed based on 10 realizations.

359 4.5.4. Facies probability distribution

360 The facies probability distribution reflects the inter variability among a set of realizations and can be
361 extracted from a probability map. Each cell in the probability map reflects the simulated category
362 probability within a set of realizations. The comparison between the distribution of the original soft
363 dataset, which constrains the simulation and the simulated facies probability distribution, allows
364 validating the performance of the simulation. Ideally the distribution of the original soft dataset is
365 reproduced by the simulation, which does not allow assumptions concerning the accuracy of the
366 allocation pattern of the simulated facies probability.

367 4.5.5. Facies probability – resistivity bias

368 The validation of the facies probability – resistivity bias depicts if the simulated facies probability
369 corresponds to the fitted curve derived from the histogram probability matching method, and thereby test
370 whether the simulated facies probability is according to the resistivity pattern. The simulated facies
371 probability value is paired with the coinciding resistivity value of the gridded SkyTEM dataset. The pairs
372 are grouped in 5 Ωm bins and the median values of simulated facies probability can be plotted for each
373 bin. Further the RMSE can be calculated between the simulated facies probability and the fitted curve at
374 each bin in order to quantify the agreement.

375 5. Results

376 5.1. TProGS setup

377 The computed transition probabilities (TP) and the fitted Markov Chain model (MCM) for both
378 horizontal and vertical direction are given in Figure 5. A sand proportion of 23% and a mean length of a
379 sand lens of 5m and 500m for vertical and horizontal direction respectively yield MCMs that are in good

380 agreement with the measured TPs. Figure 3 indicates an increasing gradient in sand proportion from north
381 to south. This non-stationary trend is also shown in Figure 5 where the additional sand-sand transition
382 MCMs are plotted that fit measured TP data from the northern and southern subdomain; defined by 13%,
383 2m, 400m and 30%, 5m and 600m respectively. 25 realizations are generated based on the MCMs that are
384 specified in Figure 5.

385 5.2. Split sample test

386 Two sets of 25 realizations are computed. The entire conditioning dataset is split into two parts, in order
387 to analyze the effect of both extremes of the conditioning spectrum: Abundant data (*onlySky20*) and
388 sparse data (*onlyBH*).

389 5.2.1. Visual comparison

390 Figure 6 presents two individual realizations (a) and (b) and the resulting probability maps (c) and (e)
391 from both conditioning datasets at an elevation of 49m. Examining the individual realizations reveals that
392 the spatial variability is much greater for the *onlyBH* scenario results. This is reasonable, because the
393 amount of constraining data is also much less. This conclusion is supported by the probability maps. The
394 probability map computed from the *onlySky20* conditioning scenario shows only little inter variability
395 among the 25 realizations and resembles almost a binary sand and clay image. The *onlyBH* scenario
396 simulates a probability map that shows high inter variability among the computed realizations, but the
397 high probable sand areas do not coincide with the high resistivity areas in the SkyTEM data (d), because
398 many large sand features are not captured by borehole data. On the other hand, some high probable sand
399 features in the *onlyBH* scenario are not represented by the *onlySky20* scenario, because small sand
400 features that are indicated by the borehole data are not detected by the SkyTEM survey.

401 5.2.2. Quantitative comparison

402 High resistivity areas are defined by a minimum resistivity value of 60 Ωm which is equivalent to 70%
403 probability of sand occurrence based on the fitted histogram curve in Figure 4. The results of the split

sample test are given in Table 1. The *onlyBH* scenario allocates only 20.1% of the high resistivity cells accordingly. Also, only 74.3% of the cells, where the lithology in the borehole reports shows sand are simulated correspondingly. Some of the borehole data are treated as soft data, which enables the simulation to overwrite the lithological information, during the SIS and the simulated quenching. This will happen especially when sand lenses are very thin and vertically confined by clay. The *onlySky20* scenario simulates 44% of those cells accordingly and allocates almost all high resistivity cells as sand. However, almost 60% of the high resistivity cells are simulated with 100% sand probability. This is in poor agreement with field data, because the fitted histogram curve does not exceed sand probability values higher than 85% (Figure 4). The SkyTEM dataset indicates a large high resistivity cluster in the south-west at an elevation of 49 m (Figure 6), which is not detected at all by the borehole dataset, because there is only one borehole penetrating this area.

5.2.3. Local comparison

Figure 7 shows the vertical profile of one borehole (99.918) that penetrates the sand cluster and compares the simulation results from the *onlyBH* and *onlySky20* scenarios. The borehole has a trust score of 95%. While both datasets agree on the top layer being sandy and the occurrence of a thick clay layer below 75 m followed by a sand layer, they disagree on the location of the deeper sand layer. In the borehole data this sand deeper sand layer is detected at an elevation of 45m and below, whereas the SkyTEM dataset indicates sand occurrence approximately 8m higher; 53m and below. This discrepancy between 45m and 53 m has considerable implications for the simulation results at 49 m shown in Figure 6. However, one borehole alone will not be sufficient to substantially influence the simulation over large areas. Marginal amplification of the *onlyBH* scenario is noticeable at borehole 99.918. On the other hand, sand probabilities are clearly amplified in the *onlySky20* scenario; everything above 0.5 is amplified close to 1.0 and everything below 0.5 close to 0. The results from Table 1 and Figures 6 and 7 support the assumption of overconditioning caused by the comprehensive cell by cell soft conditioning.

5.3. Overconditioning

429 The observed problem of overconditioning is caused by spatially correlated data which are incorporated
430 into the modeling process. A very intuitive approach to work around the problem of overconditioning is
431 decimating the SkyTEM dataset by only sampling part of it. This will only be necessary in horizontal
432 direction because the correlation length of the data is much less in the vertical direction. There is a
433 tradeoff between the correctly simulated facies probability and the accuracy of the spatial allocation
434 pattern. To illustrate this tradeoff three resampled conditioning scenarios are compiled: 100m, 200m and
435 500m sampling distance in X- and Y-direction and at the same time also including the boreholes for
436 conditioning. For each of the three conditioning scenarios (*BH-Sky100static*, *BH-Sky200static* and *BH-*
437 *Sky500static*, respectively) 25 realizations are computed and the probability maps for sand are presented
438 in Figure 8. The simulated probability maps of the *BH-Sky100static* and *BH-Sky200static* conditioning
439 scenarios are visually almost identical. Therefore only the latter is shown (d) and the image reflects
440 already a higher variability than the results by the *BH-Sky20static* scenario (c). Reducing the conditioning
441 data density increases the uncertainty of sand or clay. But at the same time the accuracy of correctly
442 locating sand or clay units decreases, because the *BH-Sky500static* scenario (e) shows high probable sand
443 areas which are not indicated by the original dataset (b). If for instance a high resistivity cell embedded in
444 low resistivity cells is sampled for the conditioning, this cell may generate a sand lens in the out thinned
445 conditioning scenario but would be limited by the neighboring cells in the *BH-Sky20static* scenario. The
446 moving sampling method can improve the spatial coverage of the conditioning datasets and thus improve
447 the quality of a set of realizations.

448 Again, the high resistivity cells are investigated to analyze if the bigger sand lenses are simulated
449 correctly by the different conditioning datasets (Table 2). It is evident that the percentage of cells at the
450 extreme ends of the simulated sand probability falls drastically after decimating the soft data out. The
451 100m distance scenarios still allocates more than 80% of the high resistivity correctly. On the other hand,
452 the *BH-Sky500static* performs poorly, by only simulating 32.7% of the high resistivity cells correctly. It is
453 also evident that the differences between static and moving sampling are small with regard to the correct
454 allocation of the higher resistivity cells.

455 5.4. Performance criteria

456 For further validation of the different sampling distances (20m, 100m, 200m and 500m) and sampling
457 schemes (static and moving) the five identified performance criteria will be applied to quantify the quality
458 of the simulations.

459 5.4.1. Sand proportion

460 Table 3 shows the defined sand proportions of the delineated glacial structure. In order to investigate non-
461 stationarities the model domain is additionally subdivided into north and south. The SkyTEM dataset
462 indicates a higher sand fraction in the southern part compared to the north, 30% and 13% respectively.
463 The simulated sand proportions for the *BH-Sky20static* scenario show a good agreement with the defined
464 values. Larger deviations are evident for the *BH-Sky200moving* scenario. Both conditioning scenarios are
465 capable of reproducing the non-stationarity of the system, in regard to the sand proportion. The sand
466 proportions are somewhat overestimated for *BH-Sky200moving* scenario, and much less for the *BH-*
467 *Sky20static* scenario. Also the overestimation of simulated sand proportion in the northern subarea is
468 larger than in the southern subarea.

469 5.4.2. Mean length

470 The comparison of the early (first lag = 100m) measured and simulated TPs for the sand-sand transitions
471 in X- and Y-direction allows to validate how well the lateral mean length is simulated by TProGS. Figure
472 9 comprises the measured TPs in horizontal direction, the fitted MCM and the computed mean TPs for
473 the *BH-Sky20static* scenario and *BH-Sky200moving* scenario, based on 10 realizations, for the total and
474 the sub-domains. The effect of overconditioning is very evident, as the computed mean TPs based on 20m
475 sampling conditioning data purely represent the original measured TP values. Since no simulation
476 freedom is present, the MCM cannot control the output. On the contrary, the *BH-Sky200moving* scenario
477 computes mean TPs that are more independent from the original data and rather follow the defined MCM.
478 The mean length of a sand lens can be derived by the steepness of the tangent where the lag approaches
479 zero. In general, the TP at lag 0 and 100 m are simulated too low; indicating that the simulated mean size

480 of a sand lens is too small. This is more prominent in results by the *BH-Sky200moving* scenario. It is
481 evident that the non-stationarity of the mean length of a sand lens is represented accordingly, although it
482 is undersimulated at all domains.

483 5.4.3. Geobody connectivity

484 For the categorized SkyTEM data θ and Γ are computed as 98.7% and 99.3%, respectively. This shows
485 values close to unity and should not be seen as a real reference, rather as a benchmark, because the
486 extreme low variability picture does not account for any uncertainties. The TProGS simulations based on
487 the two conditioning scenarios both undersimulate the connectivity metrics. The *BH-Sky20static* scenario
488 yields negative deviations of 2.1% and 1.1%, respectively and the *BH-Sky200moving* scenario 2.8% and
489 1.4%, respectively. The results indicate that θ and Γ show a similar behavior, where Γ appears to be
490 decreasingly greater as the proportion increases. Values close to unity and the very small deviations are in
491 good agreement with the general percolation theory, which sets the percolation threshold to
492 approximately 30% for 3D grids (Hovadik and Larue, 2007).

493 5.4.4. Facies probability distribution

494 Figure 10 shows the probability distribution for all discussed conditioning scenarios, with static (a) and
495 moving (b) sampling, with 25 realizations in each set. The original soft data distribution has its maximum
496 at approximately 20% and less than 5% are with either 0% or 100% sand probability. The *BH-Sky20static*
497 scenario simulates approximately 70% of the cells with zero change and thus has an extremely poor fit
498 with the soft dataset and the overconditioning is very prominent. It appears that overconditioning
499 amplifies the conditioning values to the extremes (e.g. 0.6 is simulated as 1.0 and 0.4 as 0.0, Figure 7).
500 The *BH-Sky500static* scenario reproduces the probabilities from the original soft dataset well, with only
501 approximately 10% zero change cells. However, the allocation pattern shows small resemblance with the
502 original dataset (Figure 8, (b)). *BH-Sky100static* scenario gives an intermediate solution, as the
503 probability is better reproduced than with the *BH-Sky20static* scenario, but still, more than 20% of the
504 cells are simulated as purely either sand or clay within the ensemble. Nevertheless, the *BH-Sky100static*

505 scenario is dense enough to capture the full variability of the system, as indicated by the original SkyTEM
506 dataset. Additionally the results of the *BH-Sky200static* scenario are plotted in (a). The number of zero
507 variability cells is decreased to approximately 20% and the maximum at 20% sand probability is close to
508 the original soft dataset. Figure 10, (b) compares the static with the moving sampling approach for the
509 100m and 200m distance scenarios. The simulated facies probability distribution shows no differences for
510 the static and moving 100m distance scenarios. However, at 200m sampling distance, the two sampling
511 techniques are distinguishable, as the moving sampling yields fewer zero variability cells than the static
512 sampling.

513 5.4.5. Facies probability – resistivity bias

514 The results are given in Figure 11 for the static sampling (a) and the moving sampling approach (b). The
515 strong amplification of the resulting probabilities originating from the *BH-Sky20static* scenario is obvious
516 in (a). The *BH-Sky500static* scenario performs poorly, especially in high resistivity areas, because those
517 areas are not sufficiently covered by the 500m sampling distance. A better fit is represented by the *BH-*
518 *Sky100static* scenario, because the amplification is much lower than for the *BH-Sky20static* scenario,
519 especially for high resistivity areas. On the other hand, low resistivity areas are more amplified than high
520 resistivity areas. The *BH-Sky200static* scenario gives a satisfying fit with the original fitted curve,
521 especially in high resistivity areas, which indicates that the high probable sand cells are mostly allocated
522 correctly by the model. The simulated facies uncertainty for the low resistivity cells is rather amplified
523 by the *BH-Sky200static* scenario. Figure 11, (b) investigates the simulation differences caused by the
524 static and moving sampling approach. The behaviour is similar to Figure 10, (b), because the differences
525 for the 100m distance scenarios are marginal, while the *BH-Sky200moving* scenario generates a slightly
526 lower facies probability – resistivity bias than the *BH-Sky200static* scenario. The RMSEs between the
527 fitted curve (Figure 4) and the simulations show that the *BH-Sky200moving* and *BH-Sky200static*
528 sampling conditioning scenarios perform best, both with a RMSE of 0.06. Comparable are the *BH-*
529 *Sky100moving* and *BH-Sky100static* sampling conditioning scenarios with a RMSE of 0.09 and 0.08,
530 respectively. The *BH-Sky20static* scenario performs poorest with a RMSE of 0.2.

531 6. Discussion

532 6.1. Choice of geostatistical method

533 The choice of the stochastic method for this study is application driven (Refsgaard et al., 2014). In the
534 Norsminde catchment, it is evident from both borehole and geophysical data that the glacial sequence
535 contains till clay and sand lenses distributed in extremely irregular patterns that are non-stationary.
536 Without dense conditioning data the heterogeneous and non-stationary structures will not be simulated
537 correctly. TProGS allows conditioning and operates a straight forward way to build the model of spatial
538 variability. In multi-point statistics (MPS) the definition of a reliable 3D training image is challenging,
539 especially when simulating extremely irregular patterns (Honarkhah and Caers, 2012). Defining a MPS
540 training image for the Norsminde catchment is peculiar, because it could only be based on interpreted
541 SkyTEM data; with inflated length scales in the vertical direction. This makes the model of spatial
542 variability in TProGS more reliable and objective, because it is based on measured transition probabilities
543 and not on an interpreted training image. Further the transition probabilities are based on the data type we
544 trust best: borehole data in the vertical- and SkyTEM data in the horizontal direction.

545 However, MPS is broadly applied in 2D and 3D applications: The snesim algorithm (Liu, 2006)
546 combines object-based and pixel-based methods in the general MPS framework, to enforce spatial pattern
547 reproduction and local conditioning, respectively. It was successfully applied by He et al. (2013) in a 3D
548 application. Another promising approach is given by Chugunova and Hu (2008), where MPS is tested on
549 non-stationary 2D structures, by continuous soft conditioning to a secondary variable. Here two training
550 images from the geological structure and from the secondary variable are joint in the simulation.

551 Many promising geostatistical methods have advanced to incorporate auxiliary information to constrain
552 the simulated target variable: Truncated plurigaussian simulation (Mariethoz et al., 2009a), collocated
553 simulation with probability aggregation (Mariethoz et al., 2009b). Most of them are only tested on 2D
554 applications partly with synthetic data. This present study uses TProGS as the geostatistical tool, because

555 of its reliable model of spatial variability and further it is well established in 3D applications with sparse
556 conditioning data.

557 6.2. TProGS setup

558 Direct transformation of geophysical data, such as SkyTEM, into a deterministic subsurface model is
559 risky, because too much reliance on geophysical mapping can lead to seriously wrong hydrogeological
560 models (Andersen et al., 2013). Uncertainties are expected in both, geophysical and lithological data and
561 the shape of the fitted histogram curve reflects those. High uncertainty is associated with the transition
562 zone; around 50% sand probability. Although the cut off value that divides the SkyTEM dataset into sand
563 and clay is calibrated, there is a large quantity of high uncertain cells included which make the measured
564 TPs directly dependent on the cut off value. Therefore the facies proportion and mean length are very
565 sensitive to the selection of the cut-off value. As a result, the MCM in the lateral direction, as part of the
566 TProGS setup, is highly dependent on the way the SkyTEM data is treated. Difficulties in the integration
567 of the two data types are indicated in Figure 2. Small scale heterogeneities indicated by the borehole
568 descriptions are not represented by the coarser SkyTEM dataset. This supports computing the horizontal
569 and vertical TPs individually using SkyTEM and borehole data, respectively.

570 The SkyTEM dataset used in the present study is a 3D grid of 20m x 20m x 2m which was spatially
571 interpolated from soundings with distances of about 17 m and 50-100 m along and between the flight
572 lines, respectively. To reduce the overconditioning problem it might have been preferable to use the direct
573 sounding data instead of the interpolated dataset. A similar effect is achieved by resampling, but here
574 interpolated data with a higher uncertainty than the direct soundings are used.

575 Simulating a binary system is a crude simplification of the broad range of sediments in the glacial
576 sequence. However, classifying the SkyTEM data into discrete facies or deriving the soft information on
577 facies membership are peculiar in a multi facies environment. Additionally less abundant facies (e.g.
578 gravel) will show extremely uncertain correlations in the histogram probability matching method. Last the
579 less abundant facies might be represented on a 20m domain, but it will often not be visible on the 100m

580 domain chosen for the subsequent hydrological flow simulations. Dell'Arciprete et al. (2012) present a
581 study where geostatistics are implemented to simulate small scale heterogeneities in a multi facies
582 environment.

583 6.3. Data footprint

584 Borehole and SkyTEM data are integrated by the histogram probability matching method (He et al., 2014)
585 where differences in support scale are partly neglected. The support scales of the two data types are
586 expected to vary. The lithological data from the boreholes are aggregated to 2m to be in better vertical
587 agreement with the geophysical dataset. The agreement in the lateral direction is more questionable,
588 because the footprint increases with depth for the geophysical data. The footprint is approximately 15-
589 20m on the surface and in the range of 50m at 30m penetration depth. Further the footprint will depend on
590 the material; with a larger energized volume for high conductance materials (high clay content). The two
591 steps of processing the sounding data, namely inversion and kriging are both expected to inflate the
592 footprint by smoothing values. However one can assume that the chosen grid size of 20m x 20m x 2m is
593 suitable for near surface resistivity values, because the footprint of the geophysical data is constantly
594 smaller than the correlation length, which is approximately 500m in vertical direction and 5m in lateral
595 direction.

596 6.4. Split sample test

597 Both datasources have advantages and disadvantages: Borehole data have a higher data certainty and a
598 finer spatial resolution in the vertical extent to better represent smaller sand features, but are essentially
599 undersampled in the lateral extend. On the other hand, SkyTEM data have a good spatial coverage and
600 represent the bigger sand features well, but at the same time the data are associated with a higher data
601 uncertainty. At this point, four major sources of uncertainty can be defined: (1) The inversion that
602 transforms the SkyTEM measurement into resistivity, (2) the borehole data, (3) the relationship between
603 lithology and resistivity and (4) the footprint mismatch between small scale borehole data and large scale
604 SkyTEM data. So it is precarious to assume the SkyTEM data as true geology, but it can serve as a

reference/benchmark when validating the simulation results. The *onlyBH* scenario does not capture all of the main sand features, which are revealed by the SkyTEM survey: Only 20% of the high resistivity cells, where the resistivity is greater than $70\Omega\text{m}$ are simulated correctly. For the *onlySky20* scenario only 44% of the sand descriptions in the boreholes are simulated correctly, which underlines that the SkyTEM data does not measure the finer sand features correctly. The conducted split sample test does not allow to draw firm conclusions on simulation performance, it rather analyses the agreement between the two dataset propagated through the model.

6.5. Overconditioning

Correlated data, both temporally and spatially are a common problem in hydrogeological investigations. It has not been previously reported how TProGS is able to handle such a conditioning dataset. TProGS stochastically simulates the subsurface facies system by utilizing the two mutually dependent steps SIS and simulated quenching. Soft information is not considered accordingly during the cokriging of the local probability estimate in the SIS step nor is it completely accounted for in the objective function used for the simulated quenching in the latest TProGS version. However Deutsch and Wen (2000) successfully integrate exhaustive soft data in simulated quenching, which shows that the algorithms are generally capable of incorporating soft data.

Work around methods have to be developed to overcome the problems associated with overconditioning. Decimating the soft conditioning dataset may seem as an overly simplistic and very crude approach, but the study aims at finding the balance between too few data and too many data. The risk to miss important features is high when conditioning to too few data. This study mainly deals with the latter case, where too many data lead to an underestimation of the simulation uncertainty. Including a moving sampling strategy ensures that the spatial variation in the original dataset is best represented. A drawback of this approach is that valuable information might be lost, which again underlines the need for model validation, where the entire geophysical dataset is used for the evaluation. The decimation approach works as a very pragmatic solution for a study-specific problem and

its generalization might be limited. Decimating the SkyTEM dataset out and only considering data on a 200m spaced moving sampling grid gives the most satisfying results. A 200m sampling distance is expected to be sufficient to adequately capture all relevant geological features proxied by the entire dataset; this can be argued by the fraction between the observed mean length and the conditioning spacing. The mean length of a sand lens is found to be 500m and can proxy the correlation length. With a horizontal length scale of 500m and sampling at 200m we still condition the simulation with two to three soft data points in each horizontal direction for each mean sized sand feature.

Concluding it cannot be directly concluded that overconditioning is a general problem in stochastic simulations where a vast conditioning dataset is applied. However it can be presume that heavily spatially correlated data will affect also other stochastic simulation algorithms. TProGS was clearly not developed to run with such comprehensive conditioning. To our knowledge, the problem of overconditioning has not yet been reported nor discussed and with our study we would like to create awareness. In regard to the technique of geophysical prospecting it can be concluded that the problem of overconditioning is clearly not limited to airborne based TEM data.

6.6. Performance criteria

We identified and tested five performance criteria for validating the model.

(1) *Sand proportion*. Artificial conditioning data outside the target area honoring the defined proportion and MCM may help to make the simulation more homogeneous. In that context, exhaustive hard conditioning outside the simulation target can be tested.

(2) *Mean length*. The simulated and measured TPs are compared by Carle (1997) and Carle et al. (1998). Carle et al. (1998) simulate a four category system and the simulated quenching yields a perfect match between the modeled TPs and the defined MCM. On the other hand, Carle (1997)

underlines that small deviations are to be expected and shows this by various examples where different SIS and simulated quenching parameters are tested.

(3) *Geobody connectivity*. The connectivity is partly dependent on the proportion. The sand connectivity for the simulation based on the *BH-Sky200moving* scenario is simulated lower and the sand proportion higher in comparison to the results from the *BH-Sky20static* scenario. This shows that the geobody connectivity is not fully depending on the proportion in this study. However it is a more feasible performance criterion for proportions far below the percolation threshold.

(4) *Facies probability distribution*. A good agreement between the simulated facies probability distribution and the original soft dataset doesn't ensure that the allocation pattern of the simulated probability is correct. This becomes evident when validating the results of the *BH-Sky500static* scenario.

(5) *Facies probability – resistivity bias*. The simulated facies probability should be in agreement with a corresponding resistivity observation to ensure that the spatial allocation pattern is simulated correctly. All bins are weighted the same, neglecting the inequality of data in each bin.

We used 25, 10 and 10 realizations to compute the first three performance criteria, respectively. Computing a moving average shows that the mean converges to +/-2% deviation to the final mean after ca. 15 realizations for the first criterion and after ca. 5 realizations for the second and third criteria, which justifies the selected number of realizations. The two latter criteria incorporate the computed probability map based on 25 realizations. Probability maps proved to be a useful tool to investigate the inter variability among realizations (Alabert, 1987; Carle, 2003; Mariethoz et al., 2009b). The results of the *onlyBH* scenario show the highest inter variability and a moving average tested at 10 random locations in the grid shows that after 20 realizations the mean converges to less than +/-20% from the final mean and to less than +/-10% after 23 realizations. These numbers are supposed to decrease as the conditioning data increase and therefore are 25 realizations in the analysis of the two latter criteria justifiable.

Table 4 compiles the five performance criteria for two different TProGS simulations: The *BH-Sky20static*- and the *BH-Sky200moving* scenario. A weighted and balanced analysis of the performance

679 criteria helps to identify the best result. For example, if only considering sand proportion and mean
680 length, it can be argued that the validation favors the *BH-Sky20static* scenario. However both, the facies
681 probability distribution as well as the facies probability - resistivity bias attest poor performance. On the
682 other hand, if interpreting the probability distribution only, it seems that the validation favors the *BH-*
683 *Sky500static* scenario. Collectively, the conclusion is that the *BH-Sky200moving* scenario generates the
684 overall most balanced results.

685 7. Acknowledgments

686 This work has been a part of the NiCA (Nitrate Reduction in a Geologically Heterogeneous Catchment)
687 project (www.nitrat.dk), which is funded by the Danish Council for Strategic Research.

- 689 Alabert, F., Stochastic imaging of spatial distributions using hard and soft information, *M. S. thesis*,
690 1987.
- 691 Andersen, T. R., S. E. Poulsen, S. Christensen and F. Joergensen, A synthetic study of geophysics-based
692 modelling of groundwater flow in catchments with a buried valley, *Hydrogeology Journal*, 21,
693 491-503, 2013.
- 694 Auken, E., A. V. Christiansen, J. H. Westergaard, C. Kirkegaard, N. Foged and A. Viezzoli, An
695 integrated processing scheme for high-resolution airborne electromagnetic surveys, the SkyTEM
696 system, *Exploration Geophysics*, 40(2), 184-192, 2009.
- 697 Babak, O. and C. V. Deutsch, An intrinsic model of coregionalization that solves variance inflation in
698 collocated cokriging, *Computers & geosciences*, 35(3), 603-614, 2009.
- 699 Bowling, J. C., D. L. Harry, A. B. Rodriguez and C. M. Zheng, Integrated geophysical and geological
700 investigation of a heterogeneous fluvial aquifer in Columbus Mississippi, *Journal of Applied*
701 *Geophysics*, 62(1), 58-73, 2007.
- 702 Bredehoeft, J., The conceptualization model problem--surprise, *Hydrogeology Journal*, 13(1), 37-46,
703 2005.
- 704 Caers, J., History matching under training-image-based geological model constraints, *Spe journal*, 8(3),
705 218-226, 2003.
- 706 Caers, J. and T. Zhang, Multiple-point geostatistics: a quantitative vehicle for integrating geologic
707 analogs into multiple reservoir models, *Stanford University, Stanford Center for Reservoir*
708 *Forecasting. California, USA*, 2002.
- 709 Carle, S. F., Implementation schemes for avoiding artifact discontinuities in simulated annealing,
710 *Mathematical Geology*, 29(2), 231-244, 1997.
- 711 Carle, S. F., Integration of Soft Data into Categorical Geostatistical Simulation. Not published
712 manuscript, *Water Resources Research*, 2003.
- 713 Carle, S. F. and G. E. Fogg, Transition probability-based indicator geostatistics, *Mathematical Geology*,
714 28(4), 453-476, 1996.
- 715 Carle, S. F. and G. E. Fogg, Modeling spatial variability with one and multidimensional continuous-lag
716 Markov chains, *Mathematical Geology*, 29(7), 891-918, 1997.
- 717 Carle, S. F., G. S. Weissmann and G. E. Fogg, Conditional simulation of hydrofacies architecture: A
718 transition probability approach, *SEPM Special Publication*, 1(1), 147-170, 1998.
- 719 Christiansen, A. V. and N. B. Christensen, A quantitative appraisal of airborne and ground-based
720 transient electromagnetic (TEM) measurements in Denmark, *Geophysics*, 68(2), 523-534, 2003.
- 721 Chugunova, T. L. and L. Y. Hu, Multiple-point simulations constrained by continuous auxiliary data,
722 *Mathematical geosciences*, 40(2), 133-146, 2008.

723 dell'Arciprete, D., R. Bersezio, F. Felletti, M. Giudici, A. Comunian and P. Renard, Comparison of three
724 geostatistical methods for hydrofacies simulation: a test on alluvial sediments, *Hydrogeology*
725 *Journal*, 20(2), 299-311, 2012.

726 Deutsch, C. V. and P. W. Cockerham, Practical Considerations in the Application of Simulated
727 Annealing to Stochastic Simulation, *Mathematical Geology*, 26(1), 67-82, 1994.

728 Deutsch, C. V. and A. Journel, GSLIB: Geostatistical Software Library and Users Guide, Oxford
729 University Press, New York, 1992.

730 Deutsch, C. V. and X. H. Wen, Integrating large-scale soft data by simulated annealing and probability
731 constraints, *Mathematical Geology*, 32(1), 49-67, 2000.

732 Emery, X. and J. Parra, Integration of crosswell seismic data for simulating porosity in a heterogeneous
733 carbonate aquifer, *Journal of Applied Geophysics*, 98, 254-264, 2013.

734 Falivene, O., L. Cabrera, J. A. Munoz, P. Arbues, O. Fernandez and A. Saez, Statistical grid-based facies
735 reconstruction and modelling for sedimentary bodies. Alluvial-palustrine and turbiditic examples,
736 *Geologica Acta*, 5(3), 199-230, 2007.

737 Fleckenstein, J. H., R. G. Niswonger and G. E. Fogg, River-aquifer interactions, geologic heterogeneity,
738 and low-flow management, *Ground Water*, 44(6), 837-852, 2006.

739 Giudici, M., R. Bersezio, F. Felletti, F. Baratelli, L. Cattaneo, D. dell'Arciprete, M. Mauro, P. Lorenzo
740 and V. Chiara, A multidisciplinary study of sediments' connectivity and transport parameters for
741 aquifer analogues., *Models - Repositories of Knowledge*, IAHS Publ., 355, 2012.

742 Gringarten, E. and C. V. Deutsch, Teacher's Aide Variogram Interpretation and Modeling, *Mathematical*
743 *Geology*, 33(4), 507-534, 2001.

744 Gunnink, J. and B. Siemon, Combining airborne electromagnetics and drillings to construct a stochastic
745 3D lithological model, *15th European Meeting of Environmental and Engineering Geophysics*,
746 *Dublin, Ireland*, 2009.

747 He, X., T. O. Sonnenborg, F. Jorgensen, A. S. Hoyer, R. R. Moller and K. H. Jensen, Analyzing the
748 effects of geological and parameter uncertainty on prediction of groundwater head and travel
749 time, *Hydrology and earth system sciences*, 17(8), 3245-3260, 2013.

750 He, X., J. Koch, T. O. Sonnenborg, F. Jorgensen, C. Schamper and J. C. Refsgaard, Uncertainties in
751 constructing stochastic geological models using transition probability geostatistics and transient
752 AEM data., *Water Resources Research*, 2014.

753 Hojberg, A. L. and J. C. Refsgaard, Model uncertainty - parameter uncertainty versus conceptual models,
754 *Water Science and Technology*, 52(6), 177-186, 2005.

755 Honarkhah, M. and J. Caers, Direct Pattern-Based Simulation of Non-stationary Geostatistical Models,
756 *Mathematical geosciences*, 44(6), 651-672, 2012.

757 Hovadik, J. M. and D. K. Larue, Static characterizations of reservoirs: refining the concepts of
758 connectivity and continuity, *Petroleum Geoscience*, 13(3), 195-211, 2007.

759 Hubbard, S. S. and Y. Rubin, Hydrogeological parameter estimation using geophysical data: a review of
760 selected techniques, *Journal of contaminant hydrology*, 45(1-2), 3-34, 2000.

761 Jorgensen, F., H. Lykke-Andersen, P. B. E. Sandersen, E. Auken and E. Normark, Geophysical
762 investigations of buried Quaternary valleys in Denmark: an integrated application of transient
763 electromagnetic soundings, reflection seismic surveys and exploratory drillings, *Journal of*
764 *Applied Geophysics*, 53(4), 215-228, 2003a.

765 Jorgensen, F., P. B. E. Sandersen and E. Auken, Imaging buried Quaternary valleys using the transient
766 electromagnetic method, *Journal of Applied Geophysics*, 53(4), 199-213, 2003b.

767 Jorgensen, F., P. B. E. Sandersen, E. Auken, H. Lykke-Andersen and K. Sorensen, Contributions to the
768 geological mapping of Mors, Denmark - A study based on a large-scale TEM survey, *Bulletin of*
769 *the Geological Society of Denmark*, 52, 53-75, 2005.

770 Journel, A., Beyond covariance: the advent of multiple-point geostatistics., *Geostatistics Banff. Springer*,
771 1, 225-223, 2004.

772 Kemna, A., A. Binley and L. Slater, Crosshole IP imaging for engineering and environmental
773 applications, *Geophysics*, 69(1), 97-107, 2004.

774 Krumbein, W. C. and M. F. Dacey, Markov Chains and Embedded Markov Chains in Geology,
775 *Mathematical Geology*, 1(1), 79-96, 1969.

776 Lee, S. Y., S. F. Carle and G. E. Fogg, Geologic heterogeneity and a comparison of two geostatistical
777 models: Sequential Gaussian and transition probability-based geostatistical simulation, *Advances*
778 *in Water Resources*, 30(9), 1914-1932, 2007.

779 Linde, N., J. S. Chen, M. B. Kowalsky and S. Hubbard, Hydrogeophysical parameter estimation
780 approaches for field scale characterization, SPRINGER, DORDRECHT, 2006.

781 Liu, Y. H., Using the Snesim program for multiple-point statistical simulation, *Computers &*
782 *geosciences*, 32(10), 1544-1563, 2006.

783 Mariethoz, G., P. Renard, F. Cornaton and O. Jaquet, Truncated Plurigaussian Simulations to
784 Characterize Aquifer Heterogeneity, *Ground Water*, 47(1), 13-24, 2009a.

785 Mariethoz, G., P. Renard and R. Froidevaux, Integrating collocated auxiliary parameters in geostatistical
786 simulations using joint probability distributions and probability aggregation, *Water Resources*
787 *Research*, 45, W08421, 2009b.

788 McKenna, S. A. and E. P. Poeter, Field example of data fusion in site characterization, *Water Resources*
789 *Research*, 31(12), 3229-3240, 1995.

790 Neuman, S. P., Maximum likelihood Bayesian averaging of uncertain model predictions, *Stochastic*
791 *Environmental Research and Risk Assessment*, 17(5), 291-305, 2003.

792 Refsgaard, J. C. and H. J. Henriksen, Modelling guidelines - terminology and guiding principles,
793 *Advances in Water Resources*, 27(1), 71-82, 2004.

794 Refsgaard, J. C., S. Christensen, T. O. Sonnenborg, D. Seifert, A. L. Hojberg and L. Trolborg, Review
795 of strategies for handling geological uncertainty in groundwater flow and transport modeling,
796 *Advances in Water Resources*, 36, 36-50, 2012.

797 Refsgaard, J. C., J. P. van der Sluijs, J. Brown and P. van der Keur, A framework for dealing with
798 uncertainty due to model structure error, *Advances in Water Resources*, 29(11), 1586-1597, 2006.

799 Refsgaard, J. C., E. Auken, C. A. Bamberg, B. S. Christensen, T. Clausen, E. Dalgaard, F. Effersoe, V.
800 Ernstsén, F. Gertz, A. L. Hansen, X. He, B. H. Jacobsen, K. H. Jensen, F. Joegensen, L. F.
801 Joergensen, J. Koch, B. Nilsson, C. Petersen, G. De Schepper, C. Schamper, K. I. Soerensen, R.
802 Therrien, C. Thirup and A. Viezzoli, Nitrate reduction in geologically heterogeneous catchments
803 - a framework for assessing the scale of predictive capability of hydrological models., *Science of*
804 *the Total Environment*, -(- 0), 2014.

805 Renard, P., Stochastic hydrogeology: What professionals really need?, *Ground Water*, 45(5), 531-541,
806 2007.

807 Renard, P. and D. Allard, Connectivity metrics for subsurface flow and transport, *Advances in Water*
808 *Resources*, 51, 168-196, 2013.

809 Ritzi, R. W., Behavior of indicator variograms and transition probabilities in relation to the variance in
810 lengths of hydrofacies, *Water Resources Research*, 36(11), 3375-3381, 2000.

811 Rubin, Y., X. Y. Chen, H. Murakami and M. Hahn, A Bayesian approach for inverse modeling, data
812 assimilation, and conditional simulation of spatial random fields, *Water Resources Research*, 46,
813 W10523, 2010.

814 Schamper, C. and E. Auken, SkyTEM Survey Norsminde and Lillebaek. NiCA pproject 2011,
815 *HydroGeophysics Group. Aarhus University*, 2011-06-16, 2012.

816 Seifert, D. and J. L. Jensen, Using sequential indicator simulation as a tool in reservoir description:
817 Issues and uncertainties, *Mathematical Geology*, 31(5), 527-550, 1999.

818 Seifert, D., T. O. Sonnenborg, P. Scharling and K. Hinsby, Use of alternative conceptual models to
819 assess the impact of a buried valley on groundwater vulnerability, *Hydrogeology Journal*, 16(4),
820 659-674, 2008.

821 Slater, L., Near surface electrical characterization of hydraulic conductivity: From petrophysical
822 properties to aquifer geometries - A review, *Surveys in geophysics*, 28(2-3), 169-197, 2007.

823 Sorensen, K. I. and E. Auken, SkyTEM - a new high-resolution helicopter transient electromagnetic
824 system, *Exploration Geophysics*, 35(3), 194-202, 2004.

825 Strebel, S., Conditional simulation of complex geological structures using multiple-point statistics,
826 *Mathematical Geology*, 34(1), 1-21, 2002.

827 Trolborg, L., J. C. Refsgaard, K. H. Jensen and P. Engesgaard, The importance of alternative conceptual
828 models for simulation of concentrations in a multi-aquifer system, *Hydrogeology Journal*, 15(5),
829 843-860, 2007.

830 Urish, D. W., Electrical Resistivity-Hydraulic Conductivity Relationships in Glacial Outwash Aquifers,
831 *Water Resources Research*, 17(5), 1401-1408, 1981.

832 Weissmann, G. S., S. F. Carle and G. E. Fogg, Three dimensional hydrofacies modeling based on soil
833 surveys and transition probability geostatistics, *Water Resources Research*, 35(6), 1761-1770,
834 1999.

835 Weissmann, G. S. and G. E. Fogg, Multi-scale alluvial fan heterogeneity modeled with transition
836 probability geostatistics in a sequence stratigraphic framework, *Journal of Hydrology*, 226(1-2),
837 48-65, 1999.

838 Ye, M. and R. Khaleel, A Markov chain model for characterizing medium heterogeneity and sediment
839 layering structure, *Water Resources Research*, 44(9), 2008.
840
841

Tables

Table 1. Split sample test showing how many of the high probable sand cells (resistivity > 60 Ω m) are simulated with corresponding sand probabilities (> 70%) or fully deterministic (probability = 1.0) among 25 realizations. Conditioned to onlyBH and onlySky20. The last column shows how many of the areas that are shown as sand in the boreholes are simulated with sand probabilities > 85%.

Conditioning Scenario	Prob. of sand > 0.7 AND resistivity > 60 Ωm	Prob. of sand = 1.0 AND resistivity > 60 Ωm	Prob. of sand > 0.85 AND borehole = sand
onlyBH	20.1 %	1.34 %	74.3 %
onlySky20	99.0 %	59.1%	44.0 %

Table 2. Proportion of high probable sand cells (resistivity > 60 Ωm) that are simulated with corresponding sand probabilities (> 70%) or fully deterministic (probability = 1.0) for six conditioning datasets based on 25 realizations.

Conditioning Dataset	Prob. of sand > 0.7 AND resistivity > 60 Ωm	Prob. of sand = 1.0 AND resistivity > 60 Ωm
BH-Sky20static	97.9 %	63.8 %
BH-Sky100static / BH-Sky100moving	84.1 % / 87,3	10.4 % / 10.1 %
BH-Sky200static / BH-Sky200moving	75.8 % / 71.0 %	5.4% / 3.6 %
BH-Sky500static	32.7 %	1.5 %

Table 3. Simulated and defined sand proportions for the total domain and two sub-domains based on two simulations with different soft conditioning datasets (BH-Sky20static and BH-Sky200moving), based on 25 realizations.

Mean sand proportion (%) based on 25 realizations	BH-Sky20static		
	Total	South	North
Defined	23	30	13
Simulated	25.0	30.7	13.8
Deviation	+2.0	+0.7	+1.8
BH-Sky200moving			
Defined	23	30	13
Simulated	29.3	33.7	21.5
Deviation	+6.3	+3.7	+8.5

Table 4. The five performance criteria and categorized SkyTEM data as benchmark that are applied to the two simulations with different soft conditioning datasets: Cell by cell soft conditioning and 200m moving sampling soft conditioning; both including borehole data. The first three criteria are expressed as deviation to the benchmark.

Performance Criteria	Categorized SkyTEM	BH-Sky20static	BH-Sky200moving
1. Sand proportion	23%	+2%	+6.3%
2. Mean length (X/Y)	500m	-21% / -20%	-37% / -37%
3. Geobody Connectivity (θ/Γ)	98.7% / 99.3%	-2.1% / -1.1%	-2.8% / -1.4%
4. Facies probability distribution	n.a.	Poor (approx. 70% cells with zero change)	Satisfying (approx. 15% cells with zero change)
5. Facies probability-resistivity bias	n.a.	0.20	0.06

Figure Captions

Figure 1. The study site in eastern Jutland, Dk. The Norsminde catchment with the delineated glacial structure in the western part of the catchment. Additionally the river network and the topography.

Figure 2: Side-by-side comparison of borehole lithological data and SkyTEM vertical sounding data at borehole number 99.625 (He. et. al, 2014).

Figure 3. The median resistivity values from the SkyTEM data for the 4- and 16- subarea grid. Dark colors indicate a high median (max: 43.2 Ωm and 45.0 Ωm for the 4- and 16- subarea grid, respectively), light colors a low median (min: 32.0 Ωm and 29.5 Ωm for the 4- and 16- subarea grid, respectively) and white colors the absence of data. Additionally the location of the boreholes, the river network and the delineated glacial structure. The extent is 9km in X- and 12km in Y-direction.

Figure 4. The bias corrected histogram curve: The calibrated cut off value (46 Ωm) is added to the histogram and the fitted curve is forced to honor it He et al. (2013).

Figure 5. The computed transition probabilities in vertical and horizontal direction and the fitted MCM: Vertical 5m, horizontal 500m mean length of a sand lens and 23% sand proportion. Additionally the fitted MCM for the north- and south-sub-domain are plotted for the vertical and horizontal sand-sand transitions: 2m, 400m, 13% and 5m, 600m, 30%, respectively.

Figure 6. Upper panel: Two individual realizations for two different conditioning scenarios: onlyBH (a) and onlySky20 data (b). Lower panel: Probability maps for the two scenarios c) and e) showing the probability of sand in each cell based on 25 realizations. The derived sand probability which is used for conditioning the simulation is shown in (d). All maps show data at an elevation of 49m.

Figure 7. The simulated versus the conditioned sand probability over the vertical extent at one borehole (98.918), located in the south western part of the glacial structure. The results originate from the two different soft conditioning scenarios: onlyBH and onlySky20 (based on 25 realizations each).

Figure 8. a): 100 m (small dots) and 500 m (big dots) sampling grids for thinning out the conditioning dataset; b-e): probability of sand at an elevation of 49 m for SkyTEM dataset (b), and for static 20m, 200m and 500m conditioning (c-e) Red colors represent high sand probability and blue colors low sand probability (based on 25 realizations).

Figure 9. The simulated transition probabilities for the south-, north-, and total-domain are compared with the SkyTEM data and the fitted MCM. The results for two soft conditioning dataset are shown: BH-Sky20static and BH-Sky200moving. The simulated TP and the MCM at lag 100m are compared to quantify the underestimation of a sand lens. The TP values are mean values based on 10 realizations. The defined length of a sand lens (X) and the mean simulated length for the BH-Sky20static (Y) and BH-Sky200moving scenario (Z) are given in each graph. ($X_m - Y_m / Z_m$).

Figure 10. The simulated facies probability distributions based on sets of realizations conditioned to differently sampled soft datasets (based on 25 realizations): (a) static sampling at different sampling distances and (b) stationary and moving sampling at different sampling distances. Also showing the sand probability distribution of the original soft dataset which is desired to be reproduced.

Figure 11. The simulated facies probability – resistivity bias based on sets of realizations conditioned to differently sampled soft datasets (based on 25 realizations): (a) static sampling at different sampling distances and (b) stationary and moving sampling at different sampling distances. The simulated sand probability is paired with the original resistivity value, grouped into 5 Ωm bins and then plotted as median for each bin. Also showing the observed data and the fitted curve from the histogram which is desired to be reproduced.

Figures

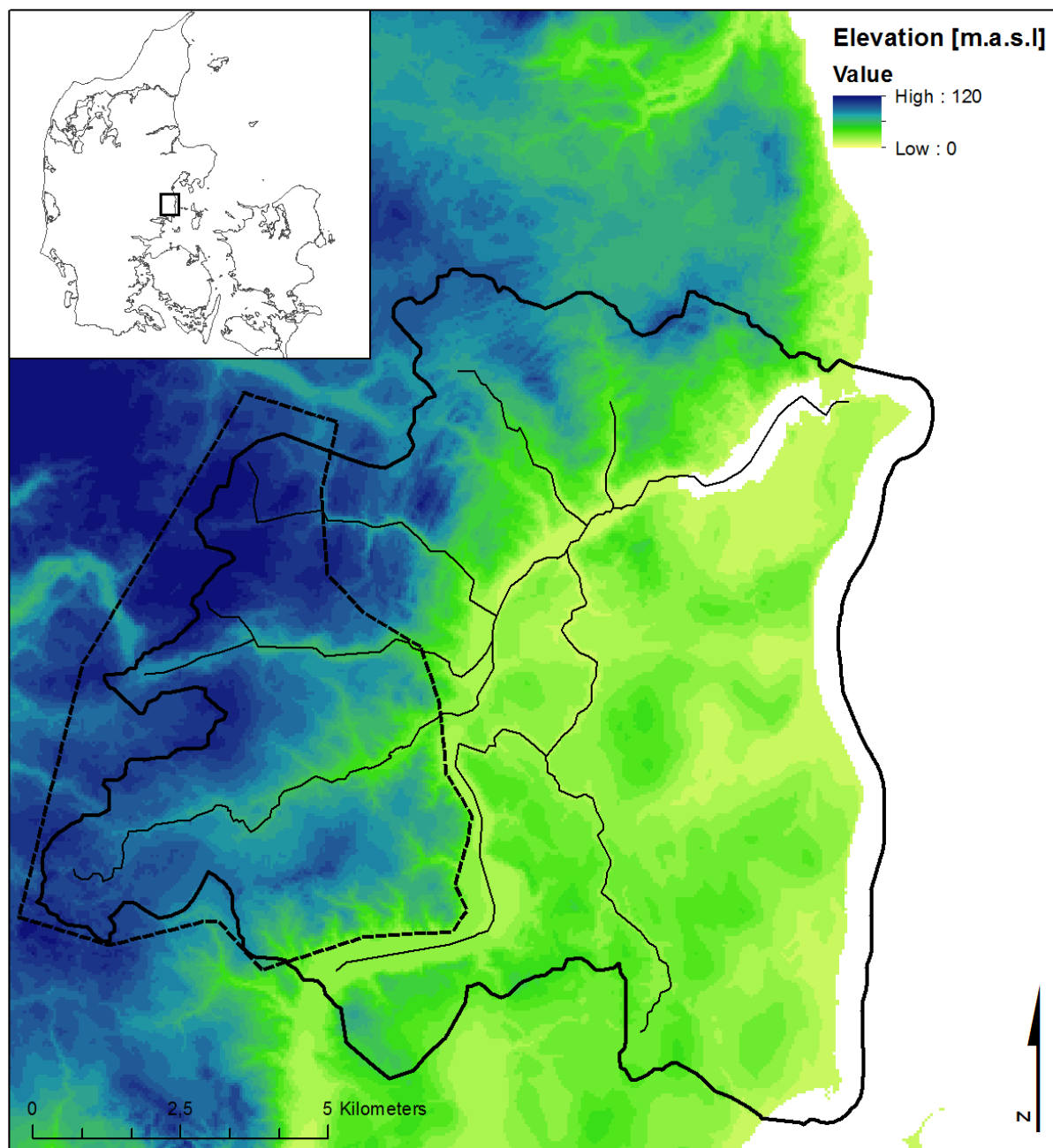


Figure 1. The study site in eastern Jutland, Dk. The Norsminde catchment with the delineated glacial structure in the western part of the catchment. Additionally the river network and the topography.

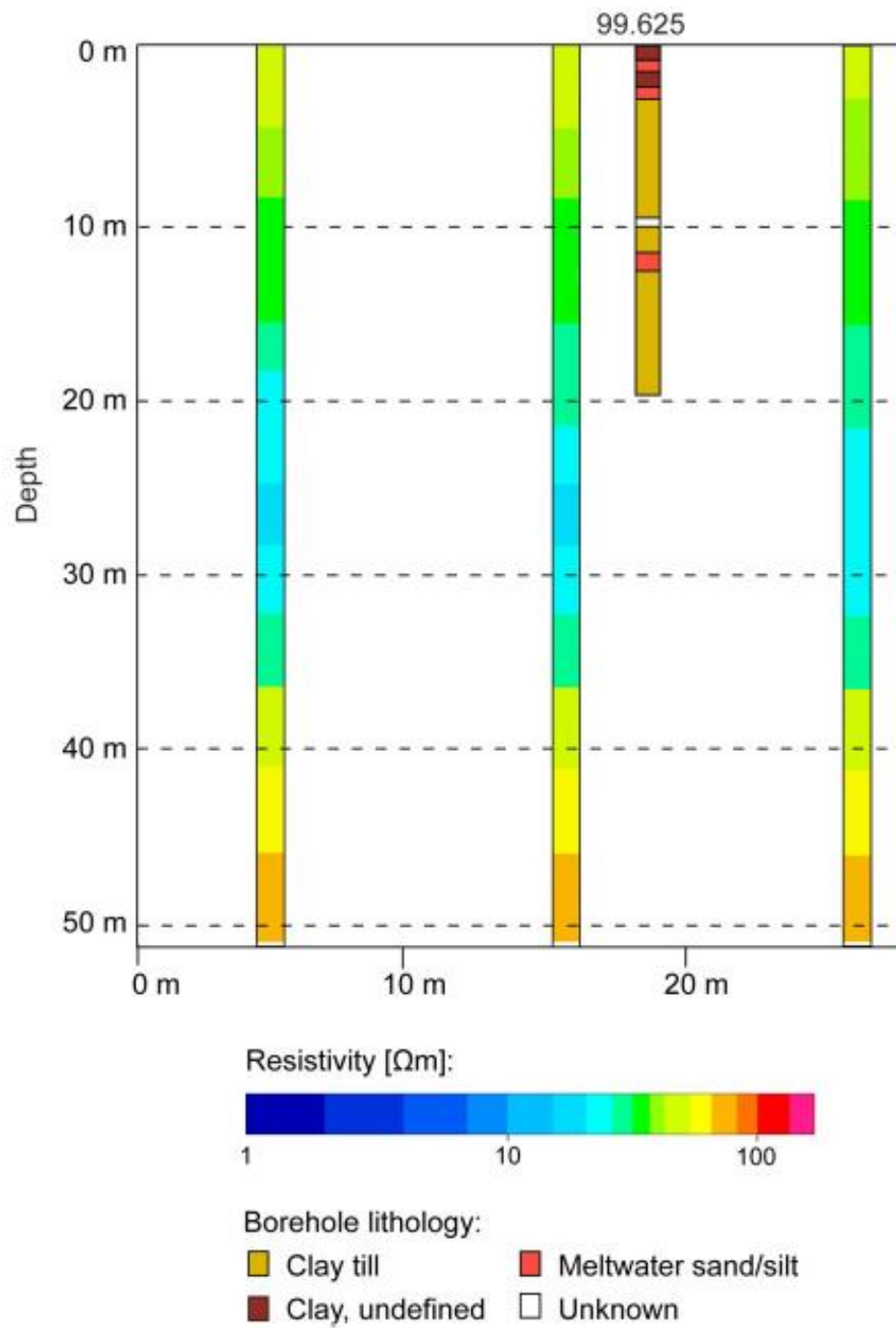


Figure 2 Side-by-side comparison of borehole lithological data and SkyTEM vertical sounding data at borehole number 99.625 (He. et. al, 2014).

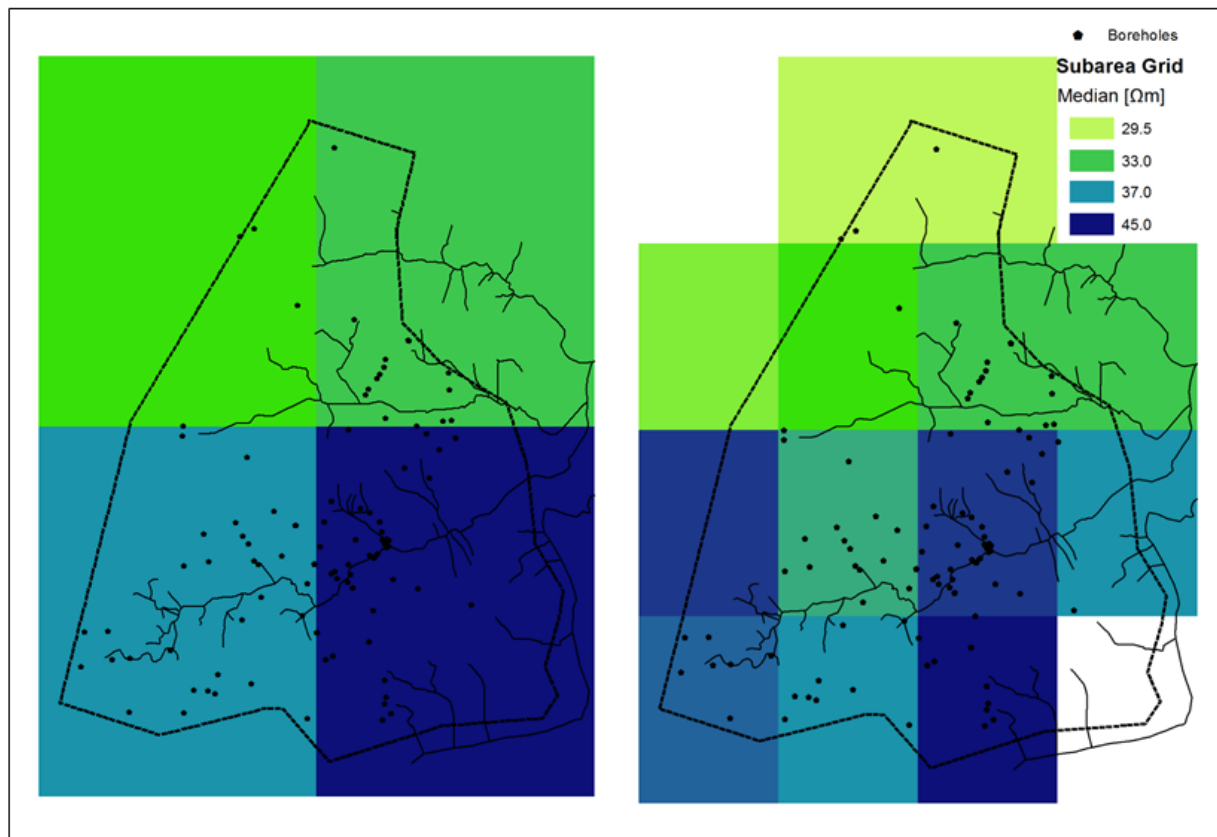


Figure 3. The median resistivity values from the SkyTEM data for the 4- and 16- subarea grid. Dark colors indicate a high median (max: 43.2 Ωm and 45.0 Ωm for the 4- and 16- subarea grid, respectively), light colors a low median (min: 32.0 Ωm and 29.5 Ωm for the 4- and 16- subarea grid, respectively) and white colors the absence of data. Additionally the location of the boreholes, the river network and the delineated glacial structure. The extent is 9km in X- and 12km in Y-direction.

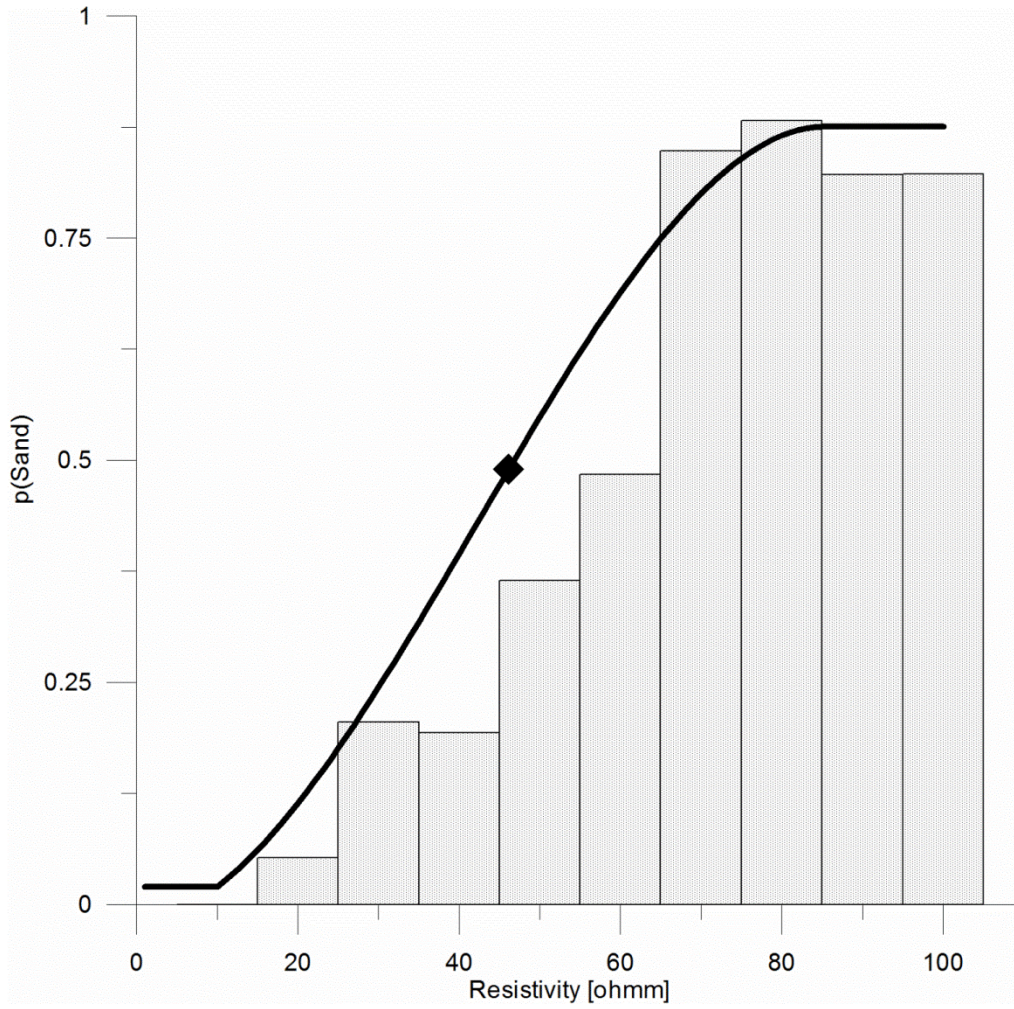


Figure 4. The bias corrected histogram curve: The calibrated cut off value (46 Ωm) is added to the histogram and the fitted curve is forced to honor it He et al. (2014).

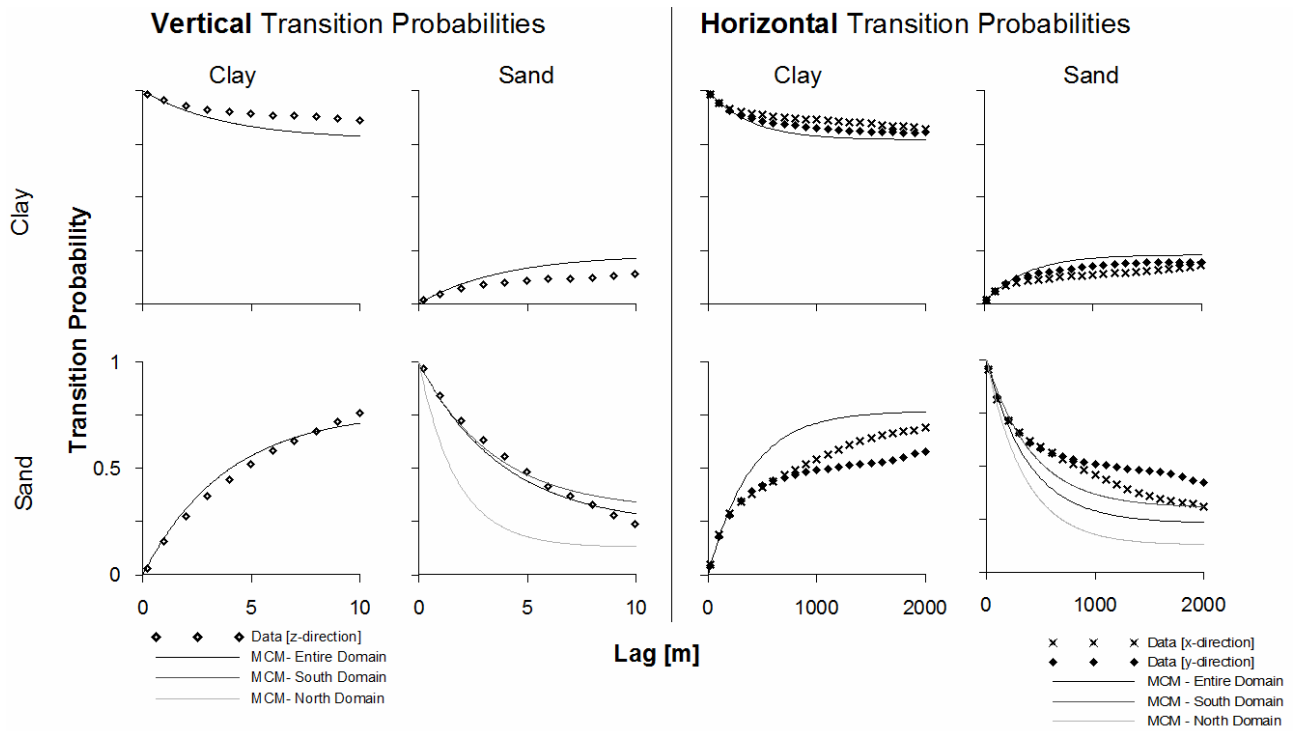


Figure 5. The computed transition probabilities in vertical and horizontal direction and the fitted MCM: Vertical 5m, horizontal 500m mean length of a sand lens and 23% sand proportion. Additionally the fitted MCM for the north- and south-sub-domain are plotted for the vertical and horizontal sand-sand transitions: 2m, 400m, 13% and 5m, 600m, 30%, respectively.

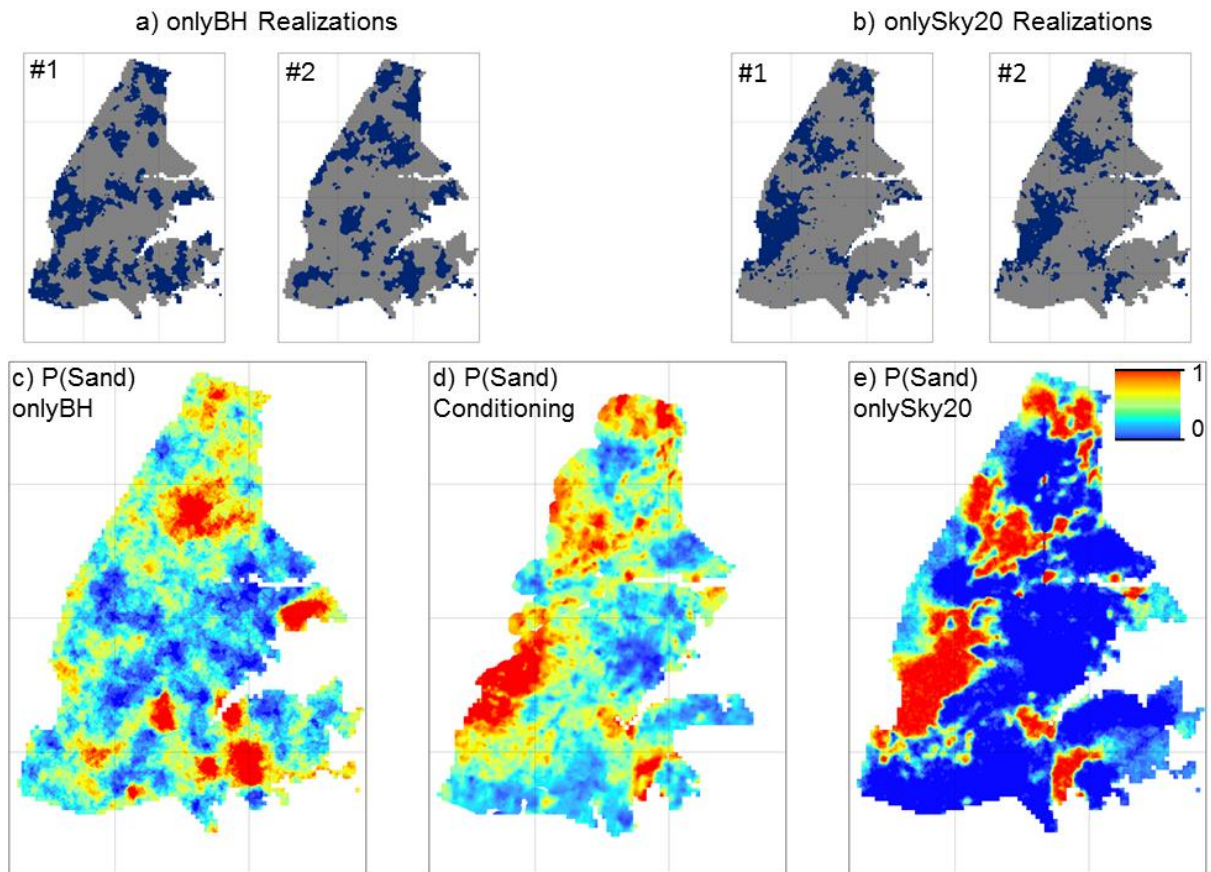


Figure 6. Upper panel: Two individual realizations for two different conditioning scenarios: *onlyBH* (a) and *onlySky20* data (b). Lower panel: Probability maps for the two scenarios c) and e) showing the probability of sand in each cell based on 25 realizations. The derived sand probability which is used for conditioning the simulation is shown in (d). All maps show data at an elevation of 49m.

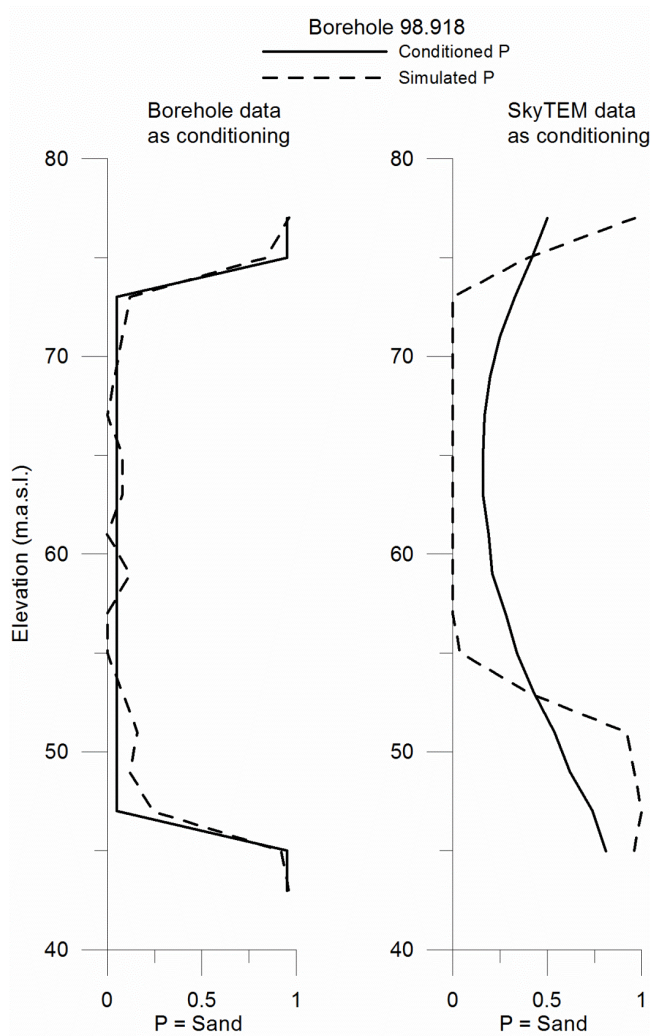


Figure 7. The simulated versus the conditioned sand probability over the vertical extent at one borehole (98.918), located in the south western part of the glacial structure. The results originate from the two different soft conditioning scenarios: *onlyBH* and *onlySky20* (based on 25 realizations each).

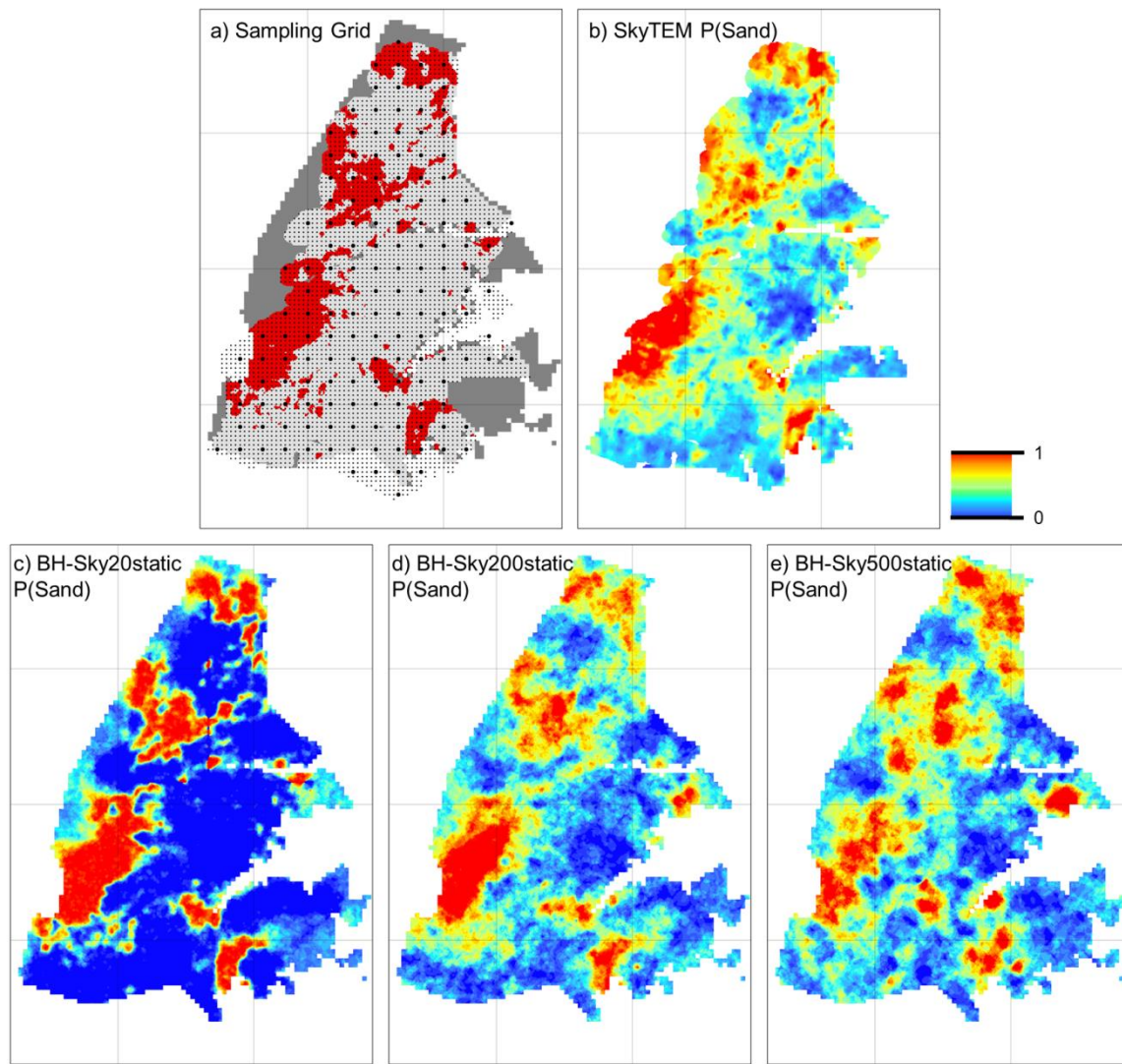


Figure 8. a): 100 m (small dots) and 500 m (big dots) sampling grids for thinning out the conditioning dataset; b-e): probability of sand at an elevation of 49 m for SkyTEM dataset (b), and for static 20m, 200m and 500m conditioning (c-e) Red colors represent high sand probability and blue colors low sand probability (based on 25 realizations).

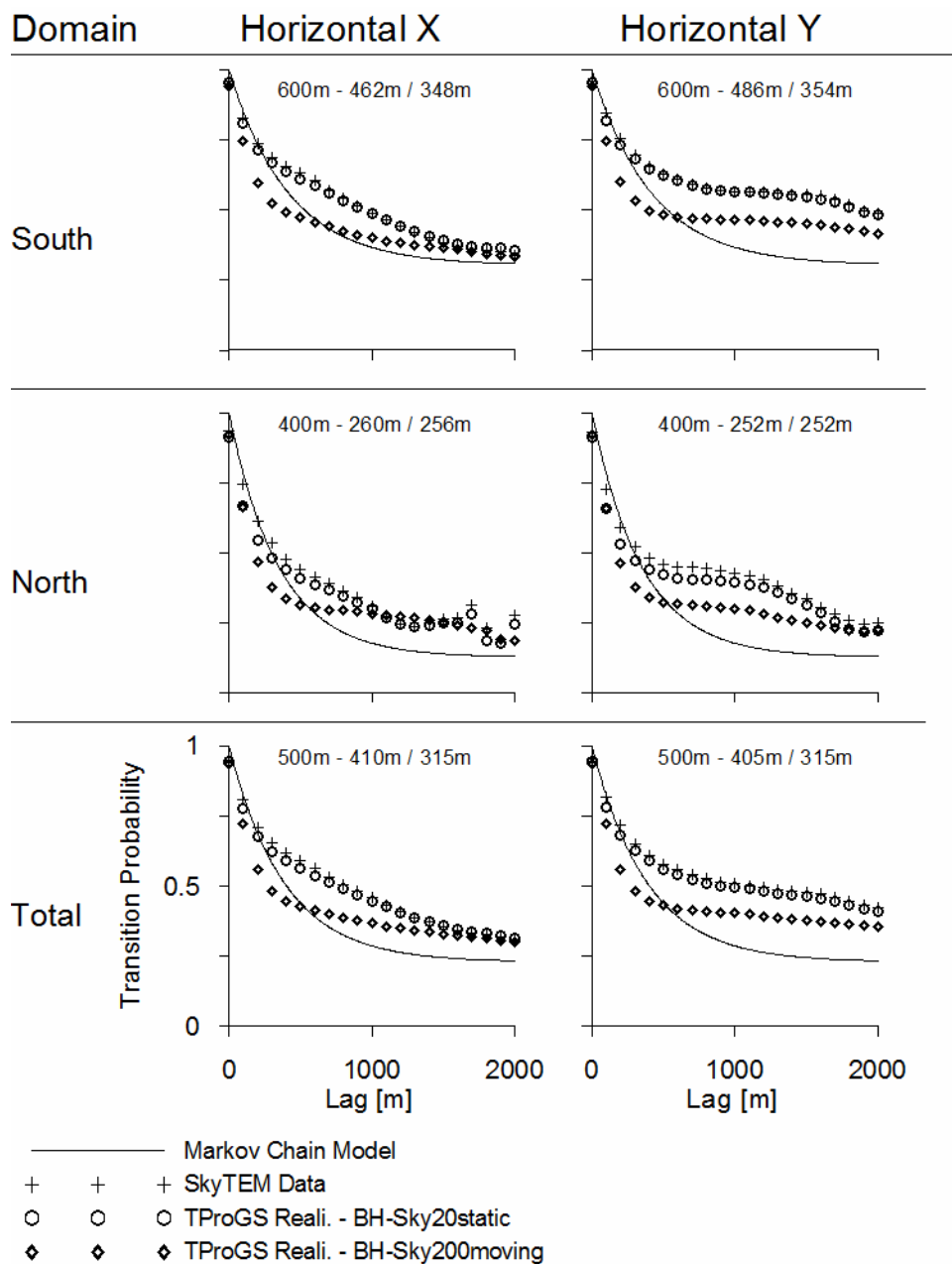


Figure 9. The simulated transition probabilities for the south-, north-, and total-domain are compared with the SkyTEM data and the fitted MCM. The results for two soft conditioning dataset are shown: *BH-Sky20static* and *BH-Sky200moving*. The simulated TP and the MCM at lag 100m are compared to quantify the underestimation of a sand lens. The TP values are mean values based on 10 realizations. The defined length of a sand lens (X) and the mean simulated length for the *BH-Sky20static* (Y) and *BH-Sky200moving* scenario (Z) are given in each graph. ($X_m - Y_m / Z_m$).

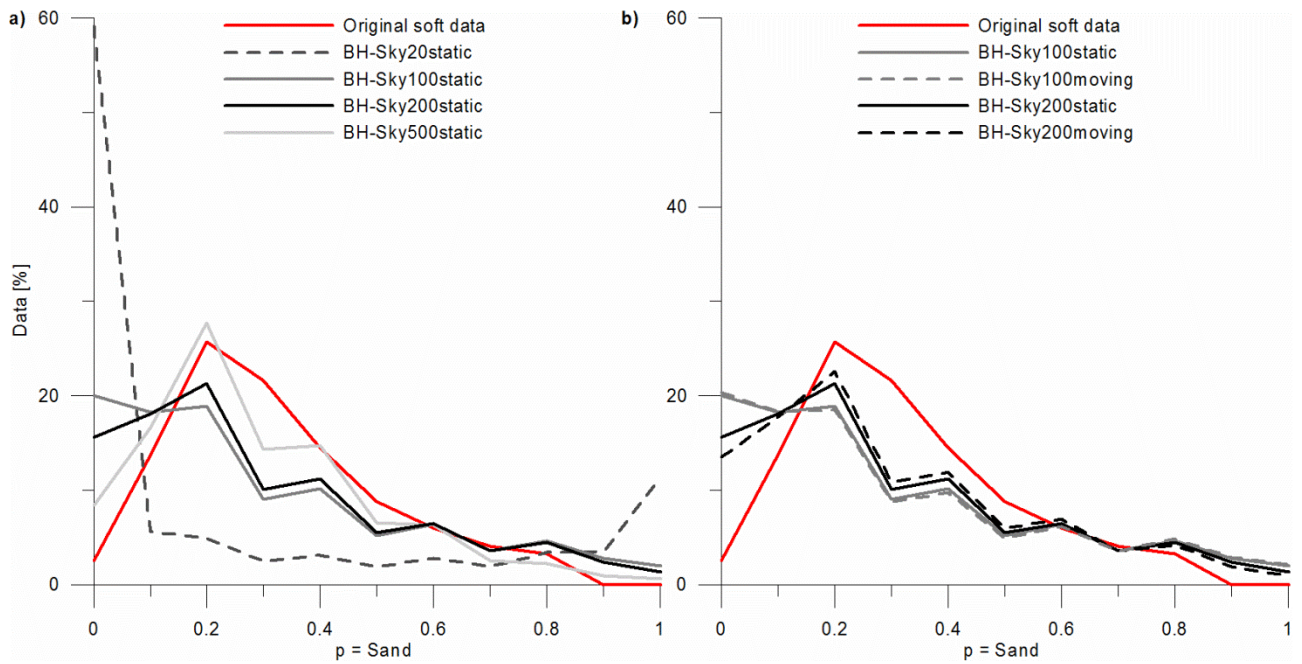


Figure 10. The simulated facies probability distributions based on sets of realizations conditioned to differently sampled soft datasets (based on 25 realizations): (a) static sampling at different sampling distances and (b) stationary and moving sampling at different sampling distances. Also showing the sand probability distribution of the original soft dataset which is desired to be reproduced.

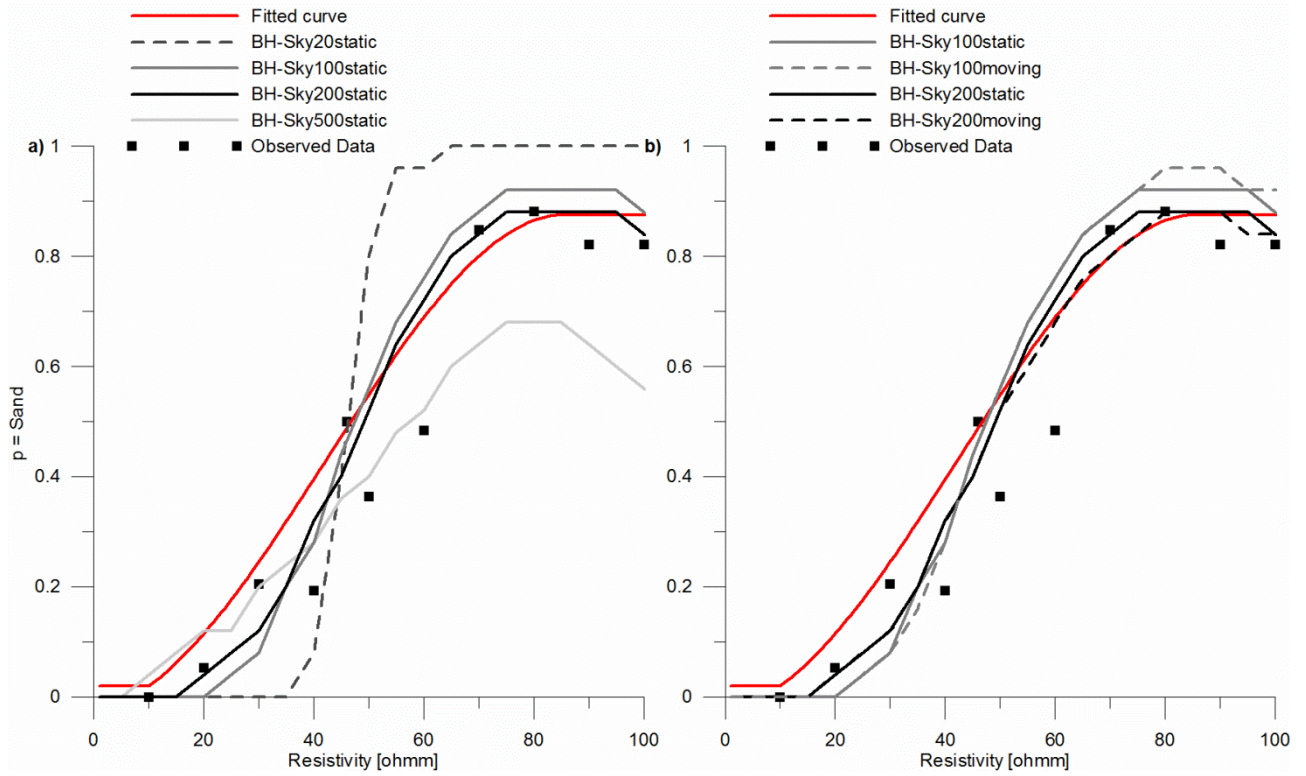


Figure 11. The simulated facies probability – resistivity bias based on sets of realizations conditioned to differently sampled soft datasets (based on 25 realizations): (a) static sampling at different sampling distances and (b) stationary and moving sampling at different sampling distances. The simulated sand probability is paired with the original resistivity value, grouped into 5 Ωm bins and then plotted as median for each bin. Also showing the observed data and the fitted curve from the histogram which is desired to be reproduced.